Stem Cell Reports
Article

ISSCR

OPEN ACCESS

HOPX Defines Heterogeneity of Postnatal Subventricular Zone Neural Stem Cells

Stefan Zweifel,[1] Guillaume Marcy,[1,3] Quentin Lo Guidice,[1] Deqiang Li,[4] Christophe Heinrich,[1] Kasum Azim,[2,5,*] and Olivier Raineteau[1,*]

[1]Université de Lyon, Université Claude Bernard Lyon 1, INSERM, Stem Cell and Brain Research Institute U1208, Bron 69500, France
[2]Brain Research Institute, University of Zurich, Zurich 8057, Switzerland
[3]Ecole Pratique des Hautes Etudes, PSL Research University, Neurogenetics Department, Paris 75014, France
[4]Department of Cell and Developmental Biology, Cardiovascular Institute, Institute for Regenerative Medicine, Perelman School of Medicine at the University of Pennsylvania, Philadelphia, PA 19104, USA
[5]Present address: Department of Neurology, Medical Faculty, Heinrich Heine University, Moorenstrasse 5, 40225 Düsseldorf, Germany
*Correspondence: kasum.azim@med.uni-duesseldorf.de (K.A.), olivier.raineteau@inserm.fr (O.R.)
https://doi.org/10.1016/j.stemcr.2018.08.006

SUMMARY

The largest diversity of neural lineages generated from the subventricular zone (SVZ) occurs early after birth and is regulated in a spatiotemporal manner depending on the expression of specific transcriptional cues. Transcriptomics and fate-mapping approaches were employed to explore the relationship between regional expression of transcription factors by neural stem cells (NSCs) and the specification of distinct neural lineages. Our results support an early priming of NSCs for the genesis of defined cell types depending on their spatial location in the SVZ and identify HOPX as a marker of a subpopulation primed toward astrocytic fates. Manipulation of HOPX expression, however, showed no effect on astrogenesis but resulted in marked changes in the number of NSCs and of their progenies. Taken together, our results highlight transcriptional and spatial heterogeneity of postnatal NSCs and reveal a key role for HOPX in controlling SVZ germinal activity.

INTRODUCTION

Germinal activity persists in the postnatal mammalian brain in specialized niches, namely the dentate gyrus (DG) of the hippocampus and the subventricular zone (SVZ) that surrounds the lateral ventricle (LV). Neural stem cells (NSCs) of the postnatal SVZ divide and give rise to transient amplifying progenitors (TAPs) that generate neuroblasts, which migrate via the rostral migratory stream (RMS) into the olfactory bulb (OB), where they differentiate into neurons (Lois and Alvarez-Buylla, 1994). The SVZ additionally generates glial progenitors that invade the local parenchyma (reviewed in Azim et al., 2016). Recently, accumulating evidence has highlighted the heterogeneous nature of postnatal SVZ in respect to different microdomains generating distinct neural lineages. For example, progenitors of GABAergic neurons are predominantly derived from the lateral SVZ (lSVZ), while the genesis of glutamatergic neuron progenitors is restricted to the dorsal SVZ (dSVZ; Azim et al., 2012; reviewed in Fiorelli et al., 2015). Furthermore, postnatally derived oligodendrocytes are generated from the dSVZ (Kessaris et al., 2006). This heterogeneity originates from early embryonic development (Fuentealba et al., 2015), and is intrinsically encoded by expression of selected transcription factors (TFs). Therefore, TFs enriched in specific embryonic forebrain regions are persistent in their expression in corresponding microdomains of the postnatal SVZ. Examples of such TFs include EMX1 (pallium; dSVZ), GSX1/2 (lateral and medial ganglionic eminence; lSVZ), and ZIC1/3 (septum; medial SVZ; reviewed in Fiorelli et al., 2015). We recently resolved the transcriptional heterogeneities of different cell populations of the postnatal SVZ, in which an unexpected large number of transcripts (i.e. 1900) were differentially expressed in NSCs and TAPs sorted from defined SVZ microdomains. Intriguingly, most of the transcriptional heterogeneity observed between the dorsal and lateral NSCs (dNSCs and lNSCs) was due to the expression of transcriptional cues. Notably, HOPX was identified with specific abundant expression in dNSCs (Azim et al., 2015). HOPX is a small (73 amino acids) atypical homeodomain protein that lacks DNA binding sites (Chen et al., 2002; Shin et al., 2002). *Hopx* expression is minimal at embryonic day 14.5 (E14.5) and peaks around E16.5 with a rostromedial to caudolateral gradient (Mühlfriedel et al., 2005). HOPX expression has been found in radial astrocytes of the adult DG, while it is described to be consistently absent from the adult SVZ (De Toni et al., 2008). Moreover, the expression of HOPX has recently received increasing attention due to its expression in quiescent NSCs, in mature astrocytes in the adult mouse DG (Li et al., 2015), as well as in outer radial glia (oRG) cells of the developing human brain (Pollen et al., 2015; Thomsen et al., 2016). Here, we used various approaches to further investigate the regionalization of the postnatal SVZ and of resident subpopulations of NSCs. In particular, we characterized the spatiotemporal and lineage-specific patterns of HOPX expression in the postnatal

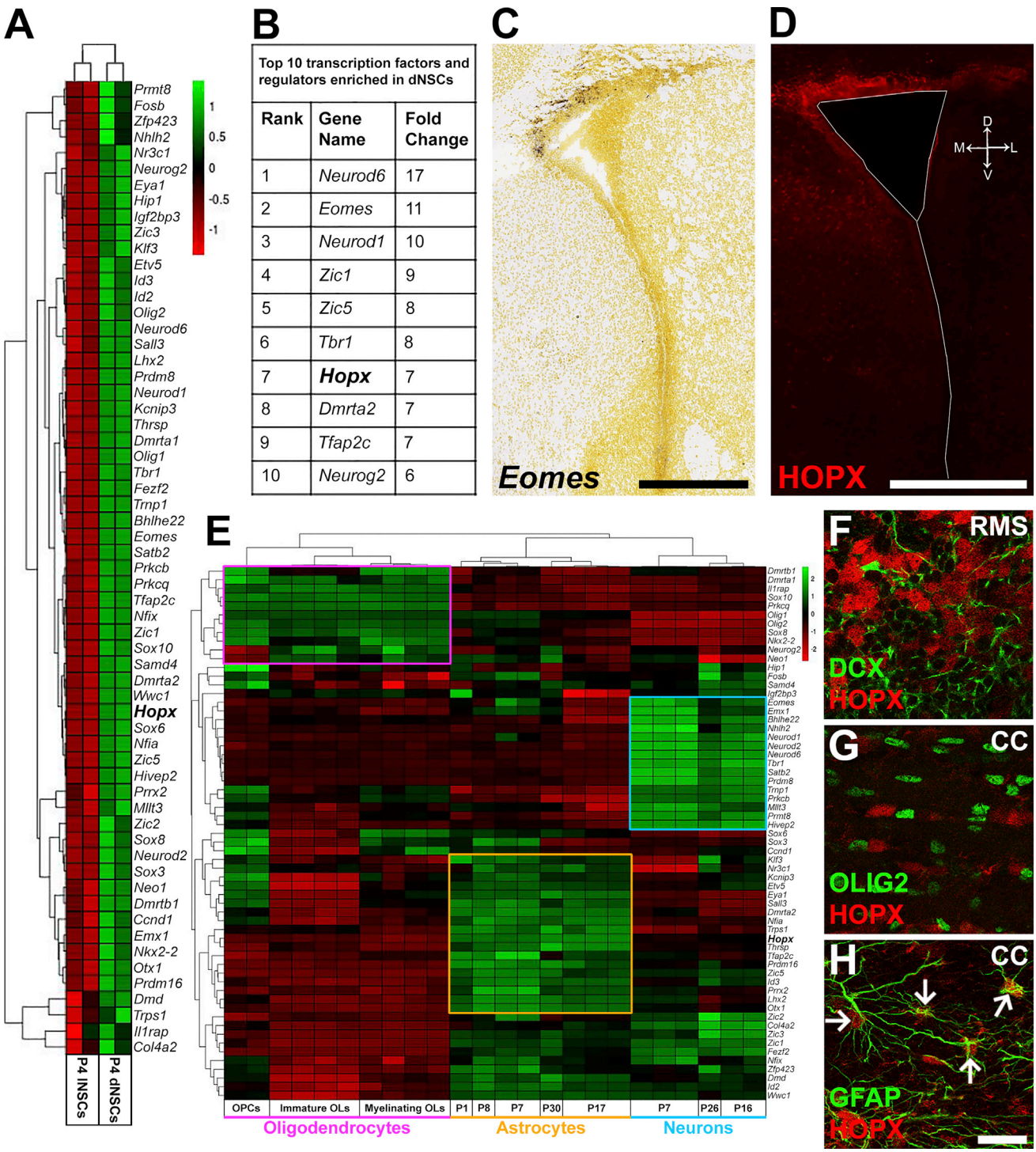

Figure 1. A Meta-Analysis of TFs Enrichment in dNSCs Highlights Their Association with Distinct Neural Lineages

(A) Heatmap showing enrichment of 61 TFs in dNSCs compared with lNSCs ($\geq$1.8-fold and $p < 0.05$).

(B) Top ten TFs enriched in dNSCs.

(C and D): Dorsal enrichment of select transcripts was confirmed using the Allen Brain Atlas for *Eomes* (C) and by immunohistochemistry for HOPX (D).

(E) Heatmap of dNSC enriched TFs reveals three clusters corresponding to defined neural lineages: oligodendrocytes (purple, 11/61); astrocytes (yellow, 18/61); neurons (turquoise, 15/61). *Hopx* (highlighted in bold) associates with the astrocytic lineage.

(legend continued on next page)

SVZ and investigated its potential function in postnatal SVZ germinal activity.

RESULTS

Hopx Is Enriched in NSCs of the dSVZ and in Cells of the Astrocytic Lineage

In a previous study, we examined the transcriptome of spatially distinct domains of the postnatal SVZ and revealed differential transcriptional networks in region-specific NSCs (Azim et al., 2015). This heterogeneity was explored further by analysis of TFs and transcriptional regulators (termed hereafter as TFs) as well as their association with defined neural lineages. Focusing on TFs only, 112 were differentially expressed between the regionalized subpopulations of NSCs (dNSCs: 61; lNSCs: 51; Figures 1A and S1A–S1C). The expression of TFs enriched dorsally was confirmed by examining *in situ* databases (http://www.brain-map.org/), and by immunohistochemistry (Figures 1C and 1D). Among transcripts enriched in dNSCs (Figure 1B), 5 out of the top 10 (*NeuroD6*, *Eomes*, *NeuroD1*, *Tbr1*, *Neurog2*) are known major determinants of the glutamatergic neuronal lineage (Schuurmans et al., 2004; Hevner et al., 2006; Brill et al., 2009; Winpenny et al., 2011). In addition, a meta-analysis was performed on publicly available datasets of isolated glial cells and neurons for the characterization of TFs into defined neural lineages (Cahoy et al., 2008). Interestingly, this analysis revealed that TFs enriched in dNSCs formed at least three clusters corresponding to astroglia (18/61), neurons (15/61), and oligodendroglia (11/61; Figure 1E). In contrast, lNSCs enriched TFs identified a single large neuronal cluster (42/51), while those of oligodendroglia were relatively fewer (3/51) and the astroglial cluster was absent (Figure S1E). These observations underline the greater diversity of lineages arising from the dSVZ, whereas the lSVZ generates almost exclusively interneurons (reviewed in Fiorelli et al., 2015; Azim et al., 2016).

We then focused our analysis onto HOPX, an atypical homeodomain protein, which was notably enriched in both dNSCs (rank 7; 7-fold enriched in dNSCs) and the astrocytic lineage (Figures 1A, 1B, 1D, and 1E). Immunodetection of HOPX confirmed that it was not expressed in migrating neuroblasts (DCX^+) of the RMS nor in $OLIG2^+$ oligodendrocytes of the corpus callosum (CC; Figures 1F and 1G). In contrast, HOPX was expressed by astrocytes in the CC (glial fibrillary acidic protein $[GFAP]^+$; Figure 1H). In the dSVZ, HOPX expression was evident in astrocyte-like lineages while absent in the other lineages (Figures S1F–S1H), in agreement with the transcriptional meta-analysis (Figure 1E). Such an expression pattern supports an early expression of HOPX and its association with the astroglial lineage.

HOPX Expression Reveals Intraregional Heterogeneity within the dSVZ

We next focused our analysis on HOPX expression within the dSVZ. Using two different antibodies, HOPX protein expression was found to be restricted to the dSVZ, while it was consistently absent from its lateral counterpart (Figure 2A; see also Figure S2). A high HOPX expression was already detectable throughout the dorsal region of the VZ/SVZ at E16. At early postnatal time points (postnatal day 1 [P1] and P4), its expression remained high but declined sharply thereafter in the young adult SVZ. Throughout its period of expression, a clear mediolateral gradient persisted, with the highest expression observed in the medial aspects of the dorsal wall and declining in its lateral aspects (i.e., high medial-to-lateral expression), which has not yet been described for any other gene (Figure 2A).

To further investigate HOPX expression within dNSCs we used the HES5:EGFP mouse line, which efficiently labels NSCs, as previously reported (Azim et al., 2015; Giachino et al., 2014). Quantification of HOPX expression in the dSVZ in this mouse line revealed that a large proportion (70.1% ± 5.0%) of $EGFP^+$ NSCs expressed HOPX. Due to the notable mediolateral gradient of HOPX expression in the dSVZ, quantifications of $EGFP^+/HOPX^+$ cells were performed in the medial and lateral subdomains. There was a significantly higher overlap in the medial subdomain of the dSVZ (90.9% ± 6.6%; dmSVZ) compared with the lateral subdomain (53.7% ± 6.2%; dlSVZ; Figure 2B). These results were confirmed by performing electroporations (EPOs) of a GFP-encoding plasmid into the dSVZ of pups, which were sacrificed 8 hr later. This enables labeling of cells in direct contact with the lumen of the ventricle, i.e., those with radial glia (RG) morphology, as previously described (Azim et al., 2015; Tiveron et al., 2017). Similar results were obtained with 76.0% ± 2.4% of the electroporated (GFP^+) cells expressing HOPX, which were significantly larger in the dorsomedial subdomain compared with its dorsolateral counterpart (93.0% ± 2.4% versus 69.3% ± 3.4%; Figure 2C).

(F–H) Confirmation of astroglial lineage-specific enrichment of HOPX by immunohistochemistry. HOPX is largely absent in neuroblasts of the RMS (DCX; F) and oligodendrocytes in the CC (OLIG2; G), but is observed in astrocytes of the CC (GFAP; H, arrows indicate double positive cells).

CC, corpus callosum; dNSC, dorsal NSCs; lNSC, lateral NSCs; RMS, rostral migratory stream; OPC, oligodendrocyte precursor cell; OL, oligodendrocyte. Scale bars, 500 μm (C and D) and 25 μm (H).

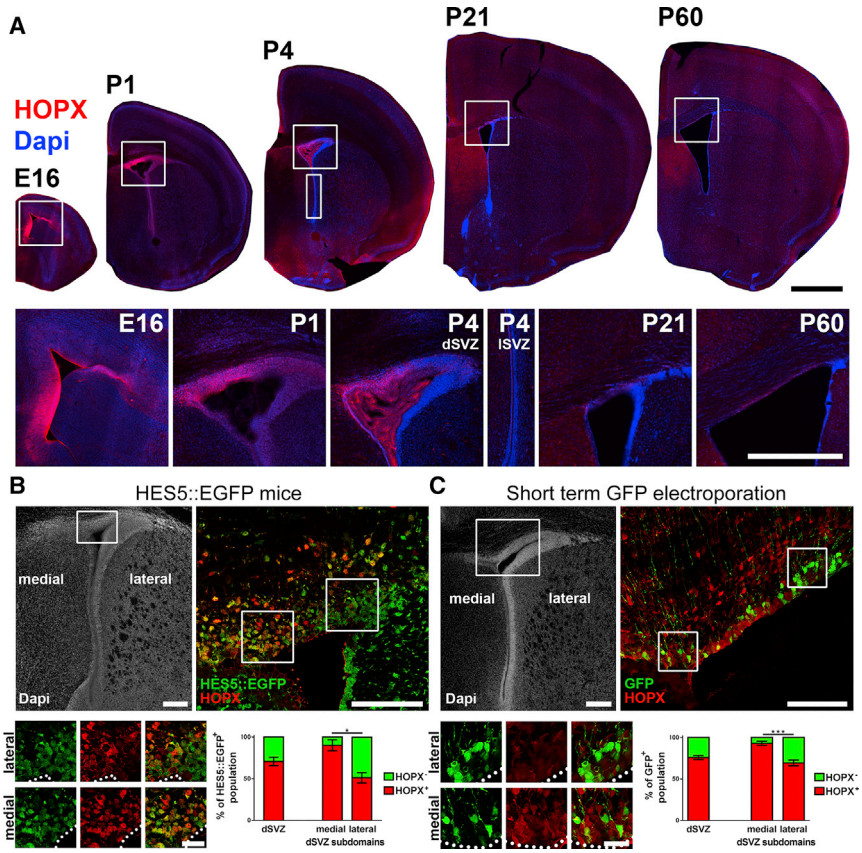

Figure 2. HOPX Exhibits a Complex Spatial and Temporal Expression Pattern within the SVZ Where it Labels a Subpopulation of dNSCs

(A) Representative micrographs of HOPX expression in coronal sections at E16, P1, P4, P21, and P60 (top panels). Higher magnifications (lower panels) show high expression in the embryo (E16) and at early postnatal stages (P1, P4) and a decline thereafter (P21, P60). A clear medial-to-lateral HOPX expression gradient is apparent in the dSVZ (see also Figure S2 for a more complete rostrocaudal overview at P4).

(B and C) Analysis of HOPX expression in dNSCs was performed in HES5:EGFP mice (B; n = 3 animals) and after short-term (8 hr) targeted EPO of a pCX-GFP plasmid (C; n = 6 animals). Crops show overlap of HOPX with HES5:EGFP- and GFP-positive cells, respectively, which was more pronounced in the medial than lateral subdomain of the dSVZ (crops and graphs).

EPO, electroporation; dSVZ, dorsal SVZ; lSVZ, lateral SVZ; dNSC, dorsal NSC. Error bars represent the SEM. Scale bars in (A) represent 1 mm (overview) and 500 μm (crops). Scale bars in (B) and (C) represent 200 μm (DAPI overview), 100 μm (higher magnification), and 25 μm (crops). *p < 0.05;***p < 0.001.

Taken together, the gradient of HOPX expression in dNSCs demonstrates intraregional NSC heterogeneity within the dSVZ wall and proposes its regulation of NSC identity and fate.

The dSVZ Is Defined by Microdomains with Distinct Lineage Outputs

Both the astrocytic expression of HOPX and its regional enrichment within a subpopulation of dNSCs suggest further transcriptional heterogeneity within the dSVZ microdomains. To test this hypothesis, we took advantage of the HES5:EGFP mice and microdissected the medial and lateral parts of the dSVZ (dmSVZ and dlSVZ, respectively) and isolated the NSCs (dmNSCs and dlNSCs, respectively) based on their EGFP expression, as previously described (Azim et al., 2015). qRT-PCR was performed to compare the expression of lineage-specific markers in regional NSC populations (Figures 3A and 3B).

We selected known transcripts enriched in NSCs as well as in defined neural lineages (Azim et al., 2015; Cahoy et al., 2008) and compared their expression levels by qPCR. Measured transcripts were all enriched in NSCs compared with the dSVZ, thereby validating our fluorescence-activated cell sorting strategy. In addition, there was no overall regional enrichment of stem cell markers (*Hes5*, *Egfp*; Basak and Taylor, 2007) and a proliferation marker (*Pcna*) within the different NSC populations, although the neuroblast marker *Dcx* was enriched in lNSCs, consistent with a greater number of neuroblasts generated by this SVZ microdomain (Yang et al., 2004; Figure 3A, top panel). Markers for the astroglial, oligodendroglial, and neuronal lineages were confirmed using the transcriptional datasets from the Barres group (Cahoy et al., 2008; Figure S3). Markers that were highly specific to astrocytes (*Aqp4*, *Aldh1l1*, *Fgfr3*, *Id3*), including *Hopx*, were enriched in dmNSCs (Figure 3B, top panel), and those for oligodendroglial lineage (*Pdgfra*, *Plp1*, *Olig1*, *Olig2*, *Dct*) were partly enriched in dmNSCs but overall more homogeneously distributed (Figure 3B, middle panel). Finally, transcripts of the neuronal lineage (*Dlx2*, *Sp8*, *Eomes*, *Vax1*, *Ebf1*) were generally enriched in dlNSCs or in lNSCs (Figure 3B, bottom panel), implying spatial segregation of lineages in the dSVZ. Taken together, *Hopx* and astroglial markers exhibit expression patterns in the dSVZ that are opposite to neuronal markers (Figure 3C). Interestingly, target genes for morphogens, i.e., WNT and SHH, showed that WNT signaling is homogenously distributed throughout the dorsal wall (*Lef1*, *Tcf7*), whereas *Gli1* is

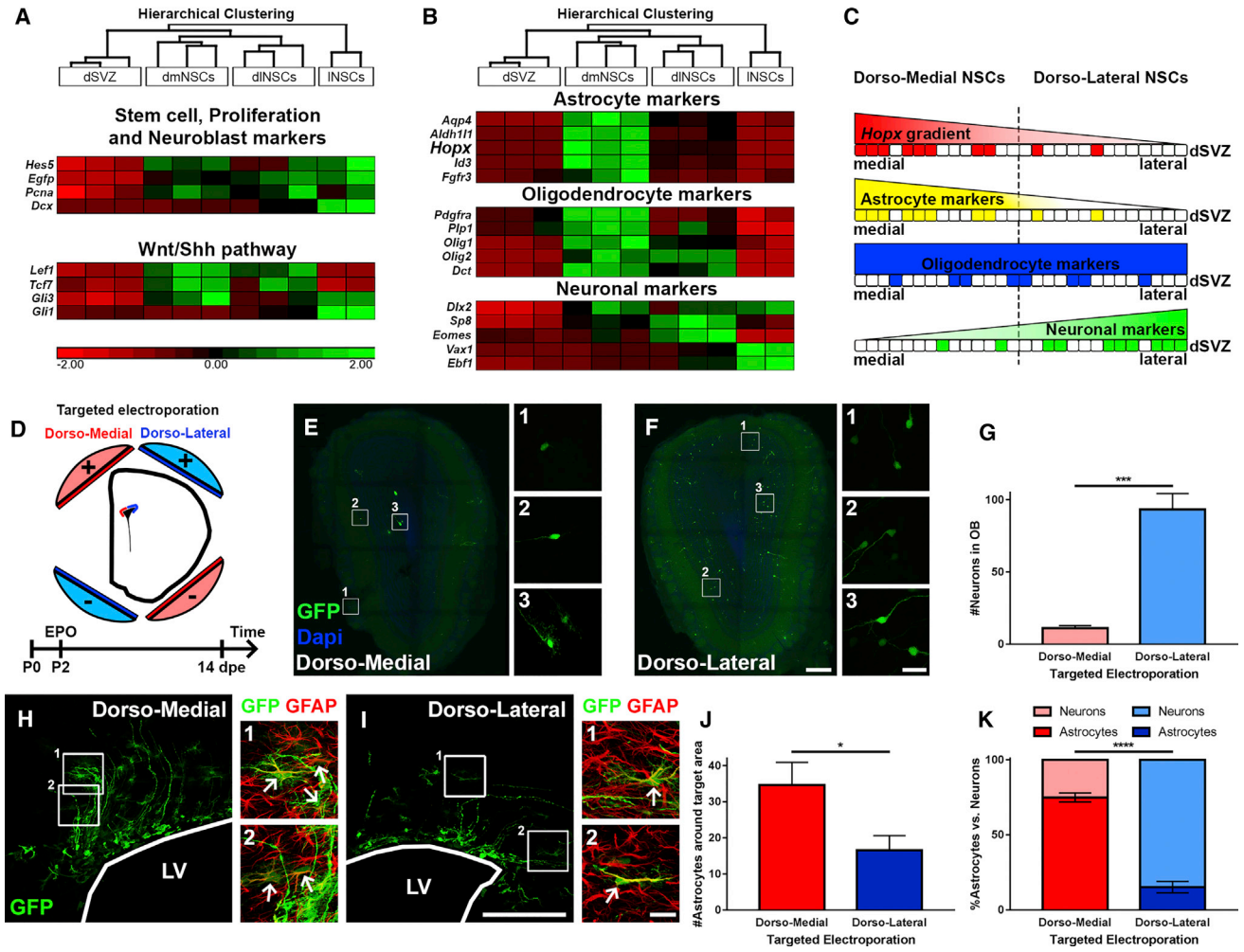

Figure 3. Lineage-Specific Markers Highlight Acquisition of Divergent Cell Fates by NSCs Located in Different dSVZ Subdomains

(A and B) Heatmaps show enrichment of transcripts in NSCs of distinct SVZ regions (dmNSCs, dlNSCs, lNSCs) compared with the dorsal environment (dSVZ). Transcripts of stem cell, proliferation, and neurogenesis markers (A; top panel) and selected signaling pathways (A; bottom panel) were analyzed. Selected markers of the astroglial (B; top panel), oligodendroglial (B; middle panel), and neuronal lineage (B; bottom panel) were analyzed. Astrocyte and neuronal markers show regional enrichment in dmNSCs and dlNSCs, respectively, while oligodendroglial markers show partial preference for enrichment in dmNSC. Note that HOPX transcripts were enriched in dmNSCs.

(C) Scheme representing the counter gradients of the expression of *Hopx* (red) and astroglial markers (yellow) against the expression of neuronal markers (green) in dNSCs. Oligodendroglial markers (blue) do not show such a clear spatial gradient.

(D) dmEPO and dlEPO highlight divergent lineage outputs of the two dorsal subdomains. The scheme shows the orientation of the electrodes for the targeted EPOs at P2 followed by analysis at 14 dpe.

(E–G) Representative micrographs of OB sections after dmEPO and dlEPO (E and F). Cell counts of OB neurons indicate that neurogenesis of the dSVZ mainly originates from dlNSCs (G).

(H–J) Representative micrographs of LV containing sections after dmEPO and dlEPO. Cells with an astrocytic fate were identified according to their morphology and GFAP expression (H and I, arrows indicate double positive cells). Quantification of astrocytes indicate that astrogenesis of the dSVZ is mainly provided by dmNSCs (J).

(K) Graph showing the fractions of astroglial and neuronal progenies from NSCs of these two subdomains. It highlights that dmNSCs are primed for generating astrocytes, whilst neurons are derived from dlNSCs.

dpe, days post electroporation; dSVZ, dorsal SVZ; dmNSCs, dorsomedial NSCs; dlNSCs, dorsolateral NSCs; lNSCs, lateral NSCs; EPO, electroporation. Animals: (A) 4–5 per n; (B) dmEPO, n = 4; (B) dlEPO, n = 5. Error bars represent SEM. Scale bars in (F) and (I) represent 200 μm (overviews) and 25 μm (crops), and apply also to (E) and (H). *p < 0.05; ***p < 0.001; ****p < 0.0001.

highly expressed in lNSCs (Figure 3A, bottom panel). Another signaling pathway target gene, *Id3*, used as a readout for bone morphogenetic protein (BMP) signaling, showed very marked enrichment in dmNSCs (Figure 3B, top panel).

Next, to test whether NSCs harbored by those two subdomains are biased to generate specific neural progenies, we performed targeted EPO of the dmSVZ and dlSVZ (Figure 3D). At a short time point (i.e., 12 hr), EPO of both microdomains with a GFP-encoding plasmid resulted in efficient GFP expression in numerous RG cells. Accurate spatial targeting was assessed by measuring the GFP fluorescence intensity within 50-μm probes distributed along the mediolateral aspects of the dSVZ at 14 days post-electroporation (dpe) (Figure S4). This confirmed the precise and reliable targeting of NSCs of the dmSVZ and dlSVZ. Both regions had given rise to large cohorts of progenies whose distribution and fate appeared to be strikingly different. Indeed, in agreement with the transcriptional profile of dlNSCs, a large population of GFP^+ neurons in the OB (93.3 ± 11.1, average number of cells/section) were found following dorsolateral EPO (dlEPO), while those derived from the dorsomedial EPO (dmEPO) remained fewer (11.1 ± 1.8; Figures 3E–3G). In contrast, the population of GFP^+ astrocytes in the vicinity of the LV (assessed by morphology and GFAP expression; Figures 3H and 3I), was substantially larger following dmEPO than dlEPO (34.6.5 ± 6.3 versus 16.5 ± 4.1; Figure 3J). Taken together, our data reveal that dmNSCs are primed to generate astrocytes (74.9% ± 3.0% astrocytes versus 25.1% ± 3.0% neurons), whilst dlNSCs generate largely olfactory neurons (15.2% ± 3.8% astrocytes versus 84.8% ± 3.8% neurons; Figure 3K).

Altogether, these findings demonstrate a high degree of heterogeneity within the dSVZ in containing specialized NSC populations that generate either astrocytes or neurons according to their location.

HOPX-Expressing dNSCs Are Biased to Acquire an Astroglial Fate

To confirm a direct relationship between HOPX expression and the generation of distinct neural lineages by dNSCs, we fate-mapped HOPX-expressing NSCs. To this end, we co-electroporated an inducible fluorescent plasmid (pFloxpA-DsRed) with an EGFP plasmid (pCX-GFP) in the dSVZ of P1 $HOPX^{CreERT2}$ mice and analyzed brain sections at 7 and 21 dpe (Figures 4A and 4B). Tamoxifen-mediated activation of the CRE-recombinase in $HOPX^+$ NSCs led to DsRed/GFP co-expression (hereafter termed dsRed) in electroporated cells and their progenies, whilst the $HOPX^-$ lineage expressed EGFP only (Figure 4C). Electroporated cell distribution and fate were assessed at both time points on serial sections encompassing the LV and the OB (Figures 4D and 4E). These results revealed the presence of $DsRed^+$ and GFP^+ cells at both 7 and 21 dpe (Figure 4F). Remarkably, while the majority of GFP^+ cells were found in the OB (7 dpe: 66.2% ± 2.1%; 21 dpe: 77.7% ± 2.5%) and acquired the typical morphology of granule neurons, the majority of $DsRed^+$ cells remained in close proximity to the dSVZ, i.e., in the CC and the cortex (7 dpe: 64.6% ± 5.6%; 21 dpe: 63.8% ± 6.8%) at both time points (Figure 4G). The distinct neural fates adopted by $HOPX^+$ or $HOPX^-$ NSCs were examined by immunolabeling of GFAP in $DsRed^+$ and GFP^+-expressing progenies in the periventricular regions at 21 dpe. This analysis confirmed that the generation of $GFAP^+$ astrocytes produced by HOPX-expressing NSCs was approximately twice as large compared with dNSCs that do not express HOPX (59.2% ± 7.1% versus 32.8% ± 4.3%, Figure 4H). These findings confirm HOPX as a marker for a subpopulation of dNSCs primed for astrogenesis.

HOPX Does Not Play an Instructive Role in Astroglial Specification of Postnatal dNSCs

To further explore the role of HOPX in regulating lineage specification and maintenance in the postnatal dSVZ, we performed loss- and gain-of-function (LoF and GoF) experiments (Figure 5A) and analyzed the effects of these manipulations on the expression of the astrocytic markers (GFAP, S100β, and fatty acid binding protein 7 [FABP7]) in the progeny of NSCs. For LoF experiments, we used $HOPX^{LacZ/WT}$ knockin mice, in which βGAL expression can be used to identify both $HOPX^{-/-}$ and $HOPX^{+/-}$ cells in homozygous ($HOPX^{LacZ/LacZ}$) and heterozygous ($HOPX^{WT/LacZ}$) mice, respectively, as validated by immunostaining (Figure S5). First, the effects of HOPX loss on astrocytes was analyzed in the CC at P19 (Figures 5B and 5C). Quantifications of S100β and/or GFAP in βGAL-expressing cells revealed no significant differences in their proportions. The majority of $βGAL^+$ cells, in both backgrounds, maintained their astrocyte identity, as revealed by their expression of GFAP (Het: 86.0% ± 2.3%; knockout [KO]: 86.7% ± 3.7%), and minimal changes in S100β expression (Figure 5C). These results are largely in agreement with those obtained by the GoF approach (Figure 5D). Indeed, although the raw numbers of $GFAP^+$ cells were increased following HOPX GoF (Figure 5E), only minor and non-significant changes in the fraction of $S100β^-/GFAP^+$ cells were observed (increase from 40.9% ± 7.1% to 56.5% ± 3.7%), whilst the other two groups ($GFAP^-/S100β^+$ and $GFAP^+/S100β^+$) were slightly decreased (Figure 5F).

To more directly address a role for HOPX in NSC specification, we performed dmEPOs of an emerald green GFP (EmGFP) transposon in an HOPX-deficient context (Figure 5G) as well as HOPX GoF in dlNSCs (Figure 5J). EPO of dmNSCs into HOPX-deficient animals was

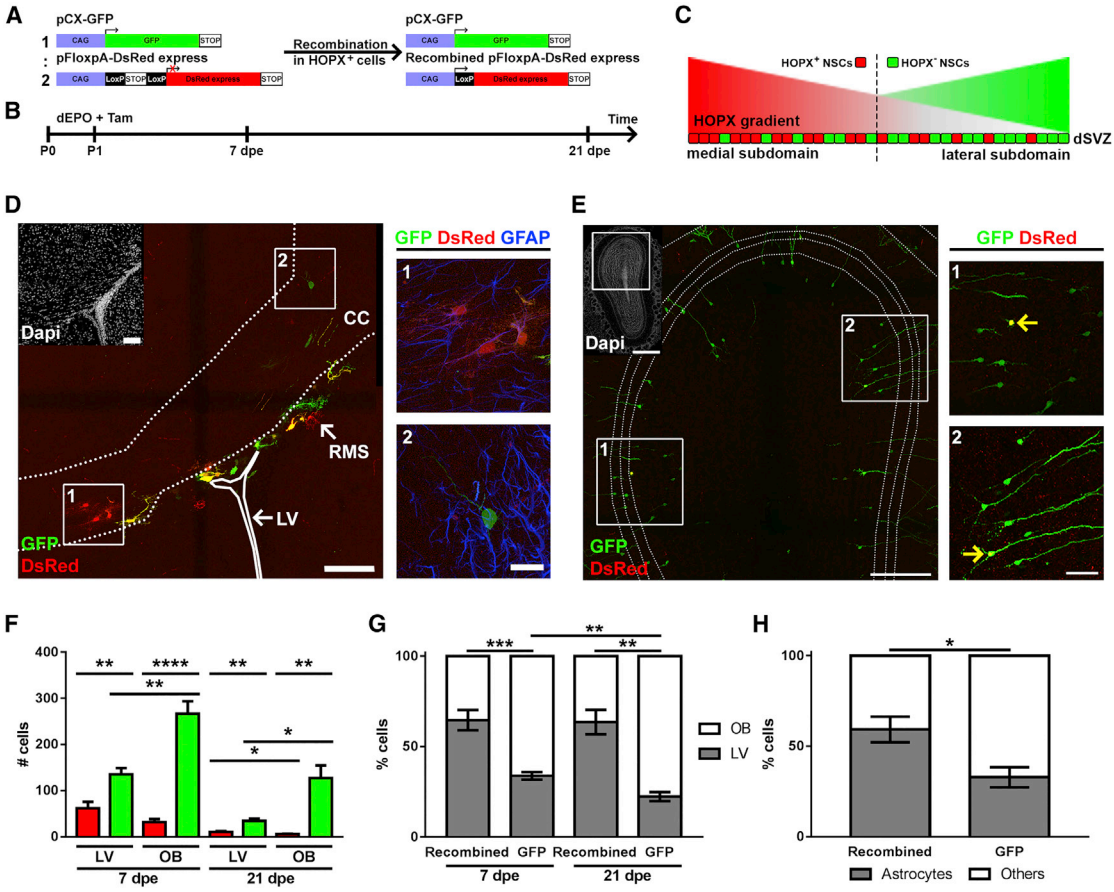

Figure 4. Conditional Fate Mapping Reveals HOPX-Expressing NSCs Are Biased to Generate Astrocytes

(A–C) Co-electroporation of a pCX-GFP and an inducible pFloxpA-DsRed plasmid (1:2; A) in HOPX^{CreERT2} mice, allows lineage tracing of HOPX^{+} and HOPX^{-} populations at short term (7 dpe) and long term (21 dpe; B). This approach results in GFP-only progenies from HOPX^{-} NSCs, whilst HOPX^{+} NSCs give rise to dsRED/GFP (termed as DsRed) progenies (C).

(D and E) Representative micrographs of an LV (D) and OB (E) section at 21 dpe. Astrocytic fate was assessed according to morphology and GFAP expression (D, crops). Neuronal fates were assessed in the OB according to morphology (E, crops; yellow arrows indicate DsRed/GFP double positive cells).

(F) Graph of absolute numbers of recombined cells (red) and GFP^{+} (green) in LV and OB sections at 7 dpe and 21 dpe.

(G) Graph showing the fractions of recombined DsRed^{+} and GFP^{+} cells harbored by LV and OB sections at 7 dpe and 21 dpe.

(H) Graph showing the fractions of cells derived from recombined DsRed^{+} and GFP^{+} populations exhibiting astrocytic traits at 21 dpe in the vicinity of the LV.

dEPO, dorsal electroporation; dpe, days post electroporation; dSVZ, dorsal SVZ; LV, lateral ventricle; NSCs, neural stem cells; OB, olfactory bulb; Tam, tamoxifen. Animals: 7 dpe, n = 5; 21 dpe, n = 4. Error bars represent SEM. Scale bars in (D) represent 100 μm (DAPI overview and fluorescence overview) and 25 μm (crops). Scale bars in (E) represent 500 μm (DAPI overview), 250 μm (fluorescence overview), and 50 μm (crops). *p < 0.05; **p < 0.01; ***p < 0.001; ****p < 0.0001.

expected to show large effects due to their high endogenous HOPX expression (see Figures 2B and 2C). Indeed, we detected decreased numbers of EmGFP^{+} progenies in the CC and cortex compared with wild-type (Figure 5H). No change in the fraction of astrocytes (assessed by glial morphology and GFAP and/or FABP7 expression) was observed (Figure 5I), indicating no changes in cell fates. Conversely, HOPX GoF was performed in dlNSCs, which endogenously express a low level or absent HOPX expression (see Figures 2B and 2C). HOPX GoF in dlNSCs was not sufficient in driving astrogenesis, as revealed by its marginal effect on GFAP^{+}/FABP7^{+} cell numbers or fraction of progenies of electroporated NSCs (Figures 5K and 5L). This suggests that dlNSCs are unable to be re-specified by HOPX GoF.

Taken together, these results indicate that HOPX does not play an instructive role astrocyte specification. The changes in the densities of GFAP^{+}-expressing cells observed

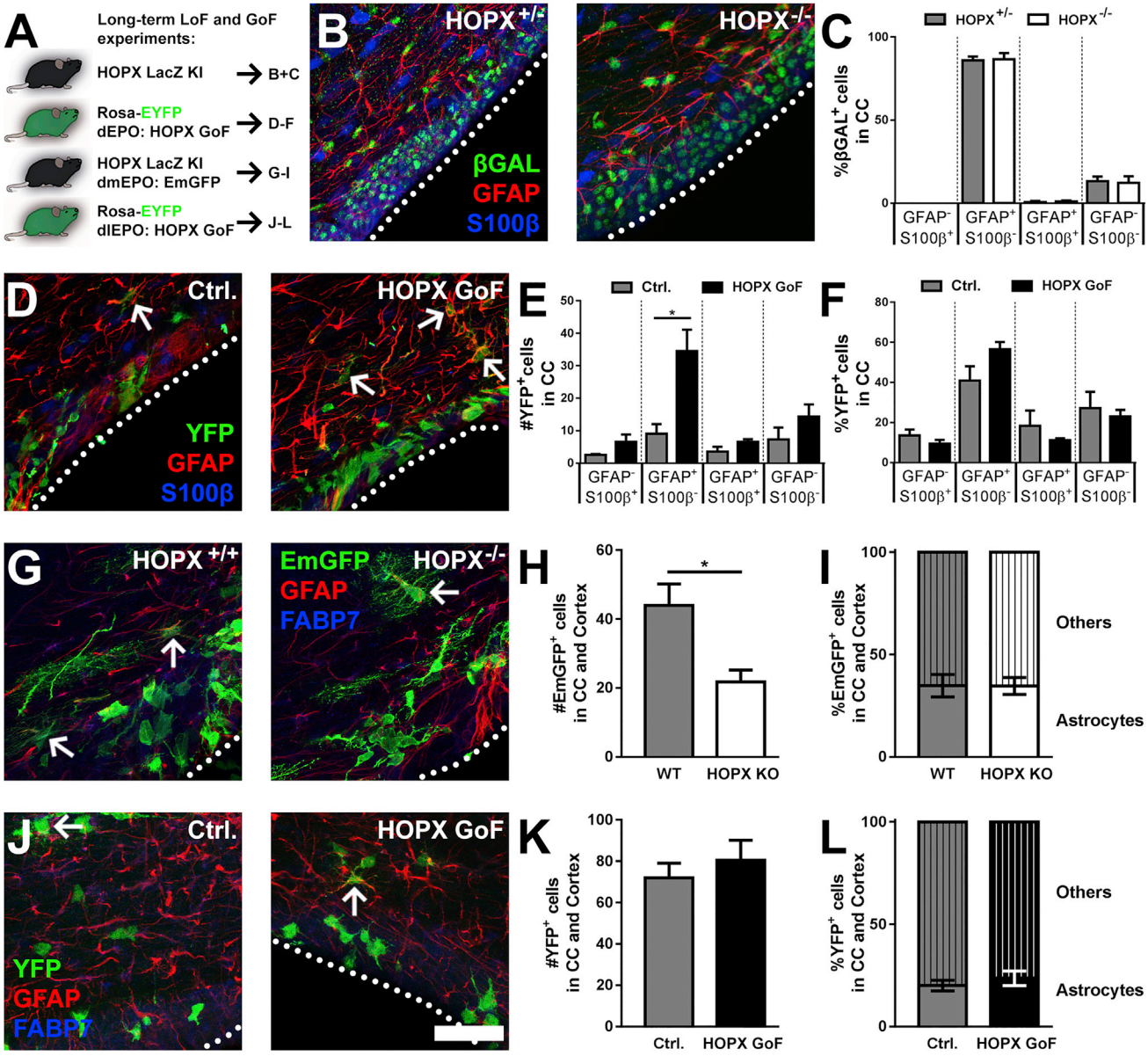

Figure 5. HOPX LoF and GoF Reveal Minimal Effects on Astroglial Specification

(A) Overview of LoF and GoF approaches.

(B and C) HOPX KO and heterozygous animals were used to analyze the βGAL$^+$ populations at P19 (B). Quantifications in the co-expression of S100β and GFAP within the βGAL population were performed in the CC. No differences in the fractions expressing S100β and/or GFAP were observed after HOPX KO (C).

(D–F) GoF experiments were performed by dEPO of pCAG-Cre and pCMV-HOPX plasmids (1:2) into Rosa-EYFP animals. Animals were sacrificed at 19 dpe. Quantifications of YFP$^+$ cells and co-expression of S100β and GFAP in the YFP populations were performed in the CC (D, arrows indicate GFAP/YFP double positive cells). Whereas the numbers of the YFP-expressing population were increased after HOPX overexpression, notably the GFAP$^+$ fraction (E), no differences in the fractions of electroporated cells expressing S100β and/or GFAP were observed (F).

(G–I) dmEPOs of pPB-CAG-EmGFP transposon plasmids were performed in WT and HOPX KO animals to closer investigate the function of HOPX during postnatal astrogenesis. Animals were sacrificed at 21 dpe (G, arrows indicate GFAP/YFP double positive cells). Analysis of EmGFP$^+$ cells was performed in the CC and cortex. Although the number of EmGFP$^+$ cells were decreased following HOPX KO (H), no change was observed in the fraction of electroporated cells expressing FABP7 and/or GFAP (I).

(legend continued on next page)

following dorsal HOPX GoF rather suggests an indirect effect through regulation of NSC stemness (i.e., persistence or expansion of the NSC population) and/or regulation of GFAP$^+$ cell survival.

HOPX Overexpression Regulates Radial Glial Cell Generation and the Germinal Activity of the dSVZ

These findings discard an instructive role of HOPX in regulating astrogenesis, but rather suggests that manipulation of HOPX alters the pool of fate-mapped cells (see above). To assess whether these effects were related to an expansion and/or persistence of NSCs, we examined the densities of dNSCs following HOPX overexpression as well as the size of their progeny at 4 dpe and 19 dpe, respectively (Figure 6A). At 4 dpe, a 2-fold increase was evident in the number of YFP$^+$ cells presenting a typical radial morphology, while non-RG-like cells were less affected (Figures 6B and 6C). At this early time point, the fraction of RG cells and non-RG cells were uniformly increased along the medial-to-lateral aspects of the dSVZ (Figure S6). In line with these findings, quantifications confirmed an increased fraction of proliferating (i.e., MCM2$^+$) RG cells at 4 dpe in the dSVZ (HOPX GoF: 73.6% ± 4.5%; Ctrl.: 60.6% ± 3.7%; Figures 6D and 6E). Remarkably, following overexpression, a minority of cells (3.5 ± 1.4 per 50-μm section) that corresponds to approximately 4% of the RG cell population showed distinctive characteristics of oRG (Figure 6G). oRG are a discrete population of ectopically located RG cells observed during corticogenesis in mice (Wang et al., 2011), and are predominant in humans. These oRG exhibited a long basal process, no apical process, and were located away from the LV surface (most of them were found in the CC) where they maintained expression of NSC markers (i.e., MCM2, SOX2; Figures 6F and 6H). A substantial fraction of HOPX-induced oRG cells maintained their proliferative potential, as revealed by the co-expression of MCM2 (63.5% ± 19.5%; Figure 6I).

To investigate the later consequences of the HOPX related expansion of RG/oRG cells, we quantified the number of YFP$^+$ cells in the dSVZ, RMS, and OB (Figures 6J–6N) at 19 dpe. At this later time point, an increased number of glial cells in the CC (Figure 5E) could be detected as well as a significant increase in the number of neurons in the OB (Figure 6N). Nevertheless, no ectopic neurons were observed in the cortex after HOPX overexpression.

Taken together, these observations demonstrate that HOPX overexpression enlarges the pool of RG cells and induces the ectopic appearance of oRG shortly following EPO, resulting in an increased output of astrocytes and neurons.

DISCUSSION

In this study, the expression hallmarks of TFs that regulate distinct neural lineages were further characterized for their enrichment in specific microdomains of the SVZ. By selecting one of these transcripts, we show that NSCs are spatially segregated and primed to differentiate toward specific neural fates. Our results identify *Hopx* as a gene that unravels further heterogeneity of the dSVZ in mediating aspects of astrogenesis and suggest its association with the emergence of germinal traits observed in higher-order mammals.

The diversity of neural subtypes generated by SVZ-NSCs after birth is much larger than first believed. The concept of SVZ regionalization whereby the genesis of distinct neural lineages are spatially and temporally regulated is being increasingly investigated (reviewed in Fiorelli et al., 2015; Azim et al., 2016). NSCs located in SVZ microdomains originate from specific regions of the developing forebrain (Fuentealba et al., 2015), and generate a large diversity of neural cells, including neuronal subtypes, depending on the expression of particular transcriptional programs. Consequently, the expression of TFs directly correlates with the acquisition of defined neural fates, a concept that was explored in the present study. We took advantage of the whole-genome transcriptome of region-specific postnatal NSCs that were recently resolved (Azim et al., 2015). A meta-analysis of TFs expressed in dorsal and lateral NSCs with datasets of isolated forebrain neuronal and glial subpopulations (Cahoy et al., 2008) highlighted transcriptional networks that correspond to microdomain-specific NSC-derived lineages. Therein, we demonstrate that NSCs are primed to acquire specific fates by the early expression of lineage-specific TFs. Such an early priming is supported by a recent single-cell RNA-sequencing characterization of adult SVZ NSCs (Llorens-Bobadilla et al., 2015).

(J–L) To investigate ectopic HOPX expression on astrogenesis in NSCs with a low/absent HOPX expression level, dlEPOs of pCAG-Cre and pCMV-HOPX plasmids (1:2) were performed in Rosa-EYFP animals. Animals were sacrificed at 21 dpe (J, arrows indicate GFAP/YFP double positive cells). Analysis of YFP$^+$ cells was performed in the CC and cortex. Neither the number of EmGFP$^+$ cells (K), nor the fraction of electroporated cells expressing GFAP and/or BLBP (L) were significantly altered following dorsolateral HOPX GoF.

βGAL, β-galactosidase; CC, corpus callosum; dEPO/dmEPO/dlEPO, dorsal/dorsomedial/dorsolateral electroporation; dpe, days post electroporation; Ctrl., control; GoF, gain-of-function; LoF, loss-of-function; KO, knockout; WT, wild-type. Animals: (C) HOPX$^{+/-}$, n = 4; (C) HOPX$^{-/-}$, n = 4; (E and F) dEPO Ctrl., n = 4; (E and F) dEPO GoF, n = 4; (H and I) HOPX$^{+/+}$ dmEPO EmGFP, n = 4; (H and I) HOPX$^{-/-}$ dmEPO EmGFP, n = 4; (K and L) dlEPO Ctrl., n = 4; (K and L) dlEPO GoF, n = 7. Error bars represent SEM. Scale bar, 50 μm. *p < 0.05.

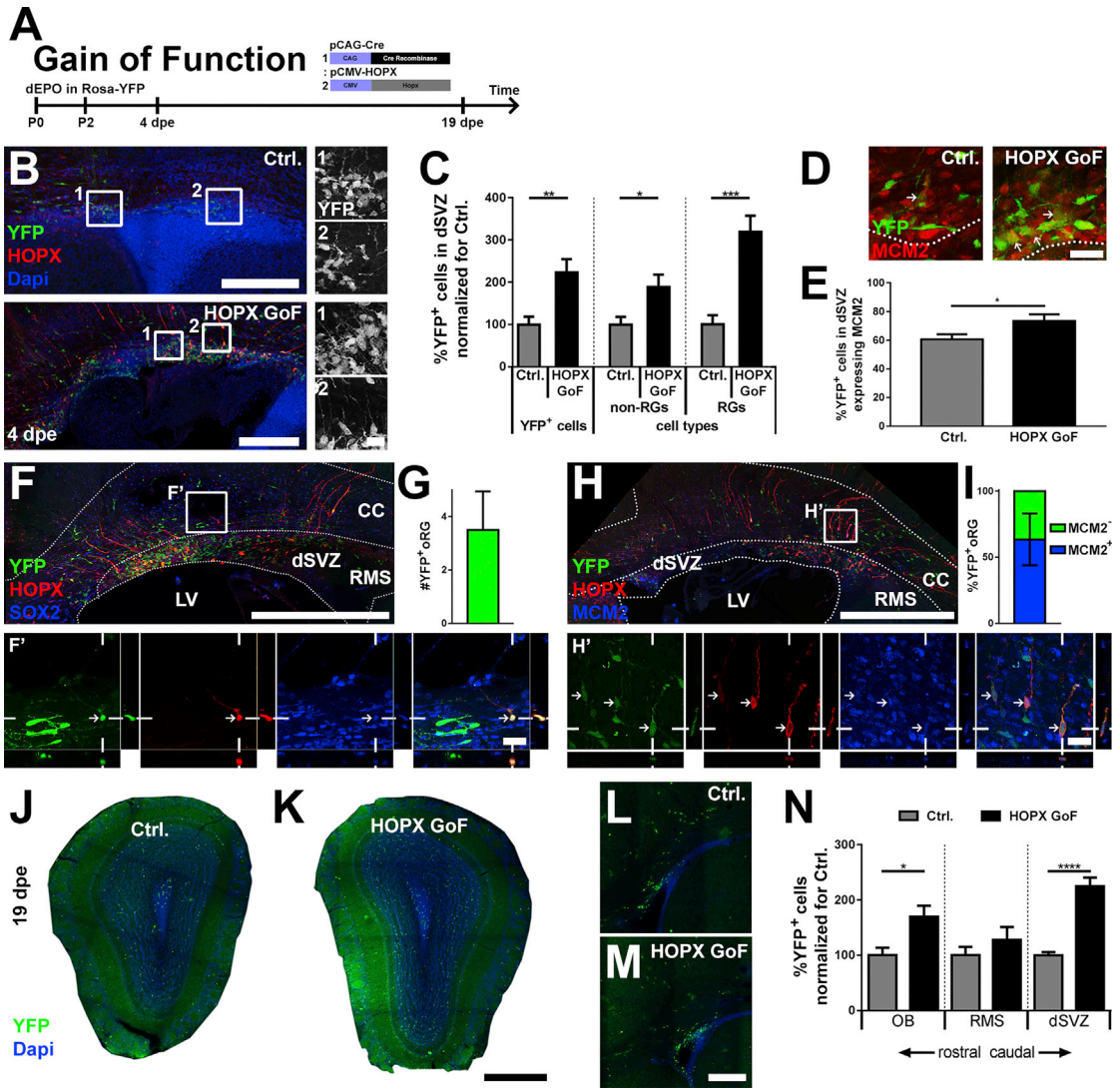

Figure 6. HOPX Overexpression Enlarges the Pool of RG Cells, Resulting in Increased Germinal Activity and Appearance of oRG Cells

(A) dEPOs of pCAG-Cre and pCMV-HOPX plasmids (1:2) into Rosa-EYFP animals were performed at P2 and quantified at 4 and 19 dpe.

(B–E) The YFP$^+$ populations were analyzed for RG morphology (B and C) and proliferative potential (D and E, arrows point to YFP/MCM2 double positive cells) at 4 dpe. The population of RG cells, but also non-RG cells were increased following HOPX overexpression (C). A higher fraction of the YFP population was positive for the proliferation marker MCM2 in the GoF group (E).

(F–I) Displaced YFP$^+$ RG cells with oRG characteristics were frequently observed 4 days following Hopx overexpression. They showed oRG morphology as well as the expression of NSC markers such as SOX2 (F) and MCM2 (H). Arrows highlight triple-positive oRG in both (F) and (H). oRG were quantified for their number per 50-μm section (G) as well as for their co-expression of MCM2 (I).

(J–N) The enlarged population of RG cells after HOPX overexpression resulted in increased overall population of YFP$^+$ cells at 19 dpe in the OB (J, K, and N) and the dSVZ (L–N).

dEPO, dorsal electroporation; dpe, days post electroporation; Ctrl., control; GoF, gain-of-function; CC, corpus callosum; dSVZ, dorsal SVZ; RMS, rostral migratory stream; LV, lateral ventricle. Animals: 4 dpe Ctrl., n = 7; 4 dpe GoF, n = 5; 19 dpe Ctrl., n = 5; 19 dpe GoF, n = 6. Error bars represent SEM. Scale bars in (B), 250 μm (overviews) and 25 μm (crop); scale bars in (D), 25 μm; scale bars in (G) and (H), 1 mm (Dapi overviews), 500 μm (fluorescence overview), and 25 μm (crops); scale bars in (K) and (M), 500 μm (also apply to J and L). *p < 0.05; **p < 0.01; ***p < 0.001; ****p < 0.0001.

Exploring the spatial heterogeneity and restricted nature of NSCs in generating specific neural lineages will be greatly facilitated by the identification of region-alized NSC markers, such as HOPX. Using two separate approaches, we demonstrate that HOPX expression is confined to a subpopulation of dNSCs whilst it is

minimally expressed in lNSCs. Additionally, our findings imply an association of HOPX with the astroglial lineage, although not supporting a direct role of HOPX in astrocyte specification. Indeed, HOPX LoF and GoF experiments revealed that it is dispensable during initial astrogenesis from dNSCs, and may modulate differentiation and acquisition of specific astrogenic traits such as GFAP expression, as previously reported elsewhere in other lineages (Obarzanek-Fojt et al., 2011). Importantly, although HOPX expression is observed in a subpopulation of NSCs that mainly produces astrocytes, it cannot be considered a pan-astrocytic marker. Indeed, HOPX expression is spatially restricted and is therefore likely to be associated with the generation of a subpopulation of astrocytes. Fate-mapping studies revealed that astrocytes are allocated to spatial domains in accordance with their embryonic sites of origin in the ventricular zone (Tsai et al., 2012). Furthermore, transcriptomic analysis of astrocytes isolated from various brain regions reveals heterogeneous expression of several astrocytic markers. For instance, HOPX was shown to be enriched in astrocytes of the dorsal forebrain (cortex and hippocampus) and lowly expressed in astrocytes of subcortical regions (thalamus and hypothalamus; Morel et al., 2017). Astrocyte heterogeneity in the CNS has recently been described to influence neuronal synaptogenesis and maturation through secretion of several extracellular matrix proteins (Eroglu and Barres, 2010). In addition, the densities of astrocytes vary greatly between brain regions (Azevedo et al., 2009). The role of HOPX in influencing regional astrocytes properties and/or densities remains to be explored.

Remarkably, postnatal HOPX overexpression enlarged the pool of RG cells and induced the appearance of a small population of ectopically located cells resembling oRG. Whilst oRG cells are rare in mice (Wang et al., 2011), their number increases dramatically in primates in forming a secondary germinal zone (i.e., the outer SVZ, or oSVZ) that contributes to the expansion of upper cortical layers during embryogenesis (Lewitus et al., 2013; Smart, 2002). Recently, a number of key studies have reported HOPX expression in human oRG (Pollen et al., 2015; Thomsen et al., 2016). Furthermore, ectopic overexpression of the hominoid-specific gene *Tbc1d3* into RG in rodents induces HOPX-expressing oRG that contribute to cortical folding (Ju et al., 2016). In line with these observations, our overexpression results suggest an instructive role for HOPX in oRG cell formation. They further reveal that ectopically generated oRG cells, together with the expansion of the RG population observed following HOPX overexpression, contribute to an increased astrocyte yield adjacent to the LV and concomitant neuronal output in the OB. As discussed above, our results further discard an instructive role of HOPX in astrocyte specification. Indeed, HOPX GoF in dlNSCs, which express low levels of HOPX and are biased to produce neurons, fail to promote astrogenesis. Conversely, loss of HOPX expression in dmNSCs does not impair astrogenesis. Thus, we propose the existence of two largely lineage-restricted dNSC populations, one predisposed toward astrogenesis and the other biased to produce neurons. The concomitant overexpression of HOPX in both populations by dEPO results in their respective expansion and therefore leads to enhanced cellular outputs, i.e., increased astrogenesis and neurogenesis, without affecting their ratio. The mechanisms by which HOPX mediates its functions remain largely unknown. HOPX is an atypical TF that does not bind to DNA directly, but modulates other TFs and/or effectors of signaling pathways at the post-transcriptional level. An interaction of HOPX with SRF has been demonstrated during cardiac development (Shin et al., 2002), but is unlikely to occur in the SVZ where SRF expression remains low (data not shown). A more likely function of HOPX is the modulation of dorsally active signaling pathways, such as the BMP and WNT pathways (see also Azim et al., 2014a; Azim et al., 2017), which have been demonstrated to fine-tune astrogenesis with neurogenesis during corticogenesis (Gross et al., 1996; Nakashima et al., 2001; Tiberi et al., 2012). Reciprocal signaling between BMP and WNT has been reported in multiple progenitor populations (He et al., 2004; Kandyba et al., 2013; Plikus et al., 2008; Song et al., 2014; Genander et al., 2014), and may be integrated by HOPX expression, as recently demonstrated in cardiomyoblasts (Jain et al., 2015). Future studies aimed at manipulating the activity of these two signaling pathways in HOPX KO animals may allow us to address these questions and investigate the role of extrinsic signal integration in lineage fate specification of neighboring populations of NSCs. It is interesting to speculate that other signaling pathways may influence the pattern of HOPX expression and may be implicated in its evolution in primates. Intriguingly, HOPX expression in the mouse SVZ follows the spatiotemporal maturation of ependymal cells, which may gradually restrict RG cell contact with the cerebrospinal fluid (Spassky et al., 2005). This, combined with the expression of HOPX in oRG, which lack apical processes in primates, suggests that an unknown cerebrospinal fluid-derived signal may regulate HOPX expression. Such signals might modulate SHH signaling that has been recently identified in regulating oRG cell formation (Wang et al., 2016). In agreement, SHH manipulation in mice results in oRG and gyri formation in the medialmost aspect of the cortex, where high HOPX expression is evident. Expression of HOPX in primate oRG might

have evolved from this original pattern of expression for the dual coupling of oRG cells and cortex expansion.

In summary, our work demonstrates that the dSVZ is much more heterogeneous than previously thought in terms of spatial segregation and early priming of NSCs in generating specific neural lineages. The abundant expression of the TF HOPX contributes to the intraregional heterogeneity of the dSVZ in rodents, whilst its overexpression suggests its association with changes observed in germinal regions throughout evolution.

EXPERIMENTAL PROCEDURES

Animals and Ethics

All animal experiments in Zurich were performed according to the Ethics Committee of the Veterinary Department of the Canton of Zurich (Approval ID 182/2011). Experiments in France were performed in accordance with European requirements 2010/63/UE and have been approved by the Animal Care and Use Committee CELYNE (APAFIS #187 & 188).

Mice used in this study were: OF1 wild-type (Charles Rivers; France), HES5:EGFP (Basak and Taylor, 2007), $HOPX^{CreERT2}$ (Takeda et al., 2011), $HOPX^{LacZ/WT}$ knockin (Shin et al., 2002), and Rosa-EYFP mice (Srinivas et al., 2001).

Plasmid Preparation and Electroporation

Plasmids used for electroporation are listed in the Supplemental Experimental Procedures. Plasmids were prepared and electroporated as previously described (Fernández et al., 2011).

Immunohistochemistry

Mice were sacrificed by an intraperitoneal overdose of pentobarbital followed by perfusion with Ringer's Lactate solution and 4% paraformaldehyde (PFA) dissolved in 0.1 M phosphate buffer (PB; pH 7.4). Brains were removed and postfixed for 12–48 hr at 4°C in 4% PFA and sectioned in 50-μm thick coronal serial sections. When necessary, antigen retrieval was performed for 20 min in citrate buffer (pH 6) at 80°C, then cooled for 20 min at room temperature and washed in 0.1 M PB. Immunostaining was performed as previously described (Azim et al., 2014b; see also Supplemental Experimental Procedures).

Fluorescence-Activated Cell Sorting and qPCR

HES5:EGFP (with C57BL/6 background) of the age P2–P4 were used for sorting for NSCs as previously described and using the exact same parameters, using 4–5 animals of one litter to generate 1 "n" number (Azim et al., 2015; see Supplemental Experimental Procedures).

Meta-Analysis of Transcriptional Profiles

To generate the lists of TFs that are enriched in dNSCs and lNSCs, we made use of previously published datasets (Azim et al., 2015; Cahoy et al., 2008), accessible on the Gene Expression Omnibus database (GEO: GSE60905 and GSE9566) and followed a procedure detailed in Supplemental Experimental Procedures.

Quantifications and Statistics

Images were acquired using a Leica DM5500 epifluorescent microscope, a Leica TCS SPE II, and a TCS SP5 confocal microscope (Leica Microsystems, Wetzlar, Germany). Images were quantified using ImageJ-win64 or assembled as representative pictures with LAS X, ImageJ, and Photoshop (CS4). Statistical analysis was done with Microsoft Excel 2013 and GraphPad Prism 7. All data are shown as mean ± SEM and statistical significance was calculated using the unpaired t test (in figures *$p < 0.05$, **$p < 0.01$, ***$p < 0.001$, ****$p < 0.0001$).

SUPPLEMENTAL INFORMATION

Supplemental Information includes Supplemental Experimental Procedures and six figures and can be found with this article online at https://doi.org/10.1016/j.stemcr.2018.08.006.

AUTHOR CONTRIBUTIONS

S.Z., K.A., and O.R. designed the study; S.Z., G.M., C.H., and K.A. performed experiments and analyses; Q.L.G. developed the heatmap generator; D.L. provided the $HOPX^{CreERT2}$ transgenic mouse line; S.Z., K.A., C.H., and O.R. wrote and edited the manuscript.

ACKNOWLEDGMENTS

The authors would like to thank Jonathan A. Epstein for kindly sharing the $HOPX^{CreERT2}$ mouse line, Verdon Taylor for sharing the HES5:EGFP mouse line, and Daniel Hohl for sharing the $HOPX^{LacZ/WT}$ knockin mouse line. Furthermore, we would like to thank Xavier Morin, Colette Dehay and Laura López-Mascaraque for providing plasmids for these experiments. We are grateful to Bruno Fischer and Anahi Hurtado-Chong for their technical assistance and Vanessa Donega for critical reading of the manuscript. This study was supported by a grant from the "Programme Avenir Lyon Saint-Etienne" and S.Z. was further supported by a Doc.Mobility fellowship from the Swiss National Science Foundation (SNF; grant number P1SKP3_168418). Other support was received from an SNF project grant NRP63 to O.R. (grant number 406340_128291) and SNF Advanced post-doc mobility fellowship to K.A. (grant number P300P3_154614).

Received: November 6, 2017
Revised: August 3, 2018
Accepted: August 5, 2018
Published: August 30, 2018

REFERENCES

Azevedo, F.A.C., Carvalho, L.R.B., Grinberg, L.T., Farfel, J.M., Ferretti, R.E.L., Leite, R.E.P., Filho, W.J., Lent, R., and Herculano-Houzel, S. (2009). Equal numbers of neuronal and nonneuronal cells make the human brain an isometrically scaled-up primate brain. J. Comp. Neurol. *513*, 532–541.

Azim, K., Fiorelli, R., Zweifel, S., Hurtado-Chong, A., Yoshikawa, K., Slomianka, L., and Raineteau, O. (2012). 3-Dimensional examination of the adult mouse subventricular zone reveals lineage-specific microdomains. PLoS One *7*, e49087.

Azim, K., Rivera, A., Raineteau, O., and Butt, A.M. (2014a). GSK3β regulates oligodendrogenesis in the dorsal microdomain of the subventricular zone via Wnt-β-catenin signaling. Glia *62*, 778–779.

Azim, K., Fischer, B., Hurtado-Chong, A., Draganova, K., Cantù, C., Zemke, M., Sommer, L., Butt, A., and Raineteau, O. (2014b). Persistent Wnt/b-catenin signaling determines dorsalization of the postnatal subventricular zone and neural stem cell specification into oligodendrocytes and glutamatergic neurons. Stem Cells *23*, 1301–1312.

Azim, K., Hurtado-Chong, A., Fischer, B., Kumar, N., Zweifel, S., Taylor, V., and Raineteau, O. (2015). Transcriptional hallmarks of heterogeneous neural stem cell niches of the subventricular zone. Stem Cells *33*, 2232–2242.

Azim, K., Berninger, B., and Raineteau, O. (2016). Mosaic subventricular origins of forebrain oligodendrogenesis. Front. Neurosci. *10*, 1–7.

Azim, K., Angonin, D., Marcy, G., Pieropan, F., Rivera, A., Donega, V., Cantù, C., Williams, G., Berninger, B., Butt, A.M., et al. (2017). Pharmacogenomic identification of small molecules for lineage specific manipulation of subventricular zone germinal activity. PLoS Biol. *15*, 1–27.

Basak, O., and Taylor, V. (2007). Identification of self-replicating multipotent progenitors in the embryonic nervous system by high Notch activity and Hes5 expression. Eur. J. Neurosci. *25*, 1006–1022.

Brill, M.S., Ninkovic, J., Winpenny, E., Hodge, R.D., Ozen, I., Yang, R., Lepier, A., Gascón, S., Erdelyi, F., Szabo, G., et al. (2009). Adult generation of glutamatergic olfactory bulb interneurons. Nat. Neurosci. *12*, 1524–1533.

Cahoy, J.D., Emery, B., Kaushal, A., Foo, L.C., Zamanian, J.L., Christopherson, K.S., Xing, Y., Lubischer, J.L., Krieg, P.A., Krupenko, S.A., et al. (2008). A transcriptome database for astrocytes, neurons, and oligodendrocytes: a new resource for understanding brain development and function. J. Neurosci. *28*, 264–278.

Chen, F., Kook, H., Milewski, R., Gitler, A.D., Lu, M.M., Li, J., Nazarian, R., Schnepp, R., Jen, K., Biben, C., et al. (2002). Hop is an unusual homeobox gene that modulates cardiac development. Cell *110*, 713–723.

Eroglu, C., and Barres, B.A. (2010). Regulation of synaptic connectivity by glia. Nature *468*, 223–231.

Fernández, M.E., Croce, S., Boutin, C., Cremer, H., and Raineteau, O. (2011). Targeted electroporation of defined lateral ventricular walls: a novel and rapid method to study fate specification during postnatal forebrain neurogenesis. Neural Dev. *6*, 13.

Fiorelli, R., Azim, K., Fischer, B., and Raineteau, O. (2015). Adding a spatial dimension to postnatal ventricular-subventricular zone neurogenesis. Development *142*, 2109–2120.

Fuentealba, L.C., Rompani, S.B., Parraguez, J.I., Obernier, K., Romero, R., Cepko, C.L., and Alvarez-buylla, A. (2015). Embryonic origin of postnatal neural stem cells article embryonic origin of postnatal neural stem cells. Cell *161*, 1644–1655.

Genander, M., Cook, P.J., Ramsköld, D., Keyes, B.E., Mertz, A.F., Sandberg, R., and Fuchs, E. (2014). BMP signaling and its pSMAD1/5 target genes differentially regulate hair follicle stem cell lineages. Cell Stem Cell *15*, 619–633.

Giachino, C., Basak, O., Lugert, S., Knuckles, P., Obernier, K., Fiorelli, R., Frank, S., Raineteau, O., Alvarez-Buylla, A., and Taylor, V. (2014). Molecular diversity subdivides the adult forebrain neural stem cell population. Stem Cells *32*, 70–84.

Gross, R.E., Mehler, M.F., Mabie, P.C., Zang, Z., Santschi, L., and Kessler, J.A. (1996). Bone morphogenetic proteins promote astroglial lineage commitment by mammalian subventricular zone progenitor cells. Neuron *17*, 595–606.

He, X.C., Zhang, J., Tong, W.-G., Tawfik, O., Ross, J., Scoville, D.H., Tian, Q., Zeng, X., He, X., Wiedemann, L.M., et al. (2004). BMP signaling inhibits intestinal stem cell self-renewal through suppression of Wnt-β-catenin signaling. Nat. Genet. *36*, 1117–1121.

Hevner, R.F., Hodge, R.D., Daza, R.A., and Englund, C. (2006). Transcription factors in glutamatergic neurogenesis: conserved programs in neocortex, cerebellum, and adult hippocampus. Neurosci. Res. *55*, 223–233.

Jain, R., Li, D., Gupta, M., Manderfield, L.J., Ifkovits, J.L., Wang, Q., Liu, F., Liu, Y., Poleshko, A., Padmanabhan, A., et al. (2015). Integration of Bmp and Wnt signaling by Hopx specifies commitment of cardiomyoblasts. Science *348*, aaa6071.

Ju, X.C., Hou, Q.Q., Sheng, A.L., Wu, K.Y., Zhou, Y., Jin, Y., Wen, T., Yang, Z., Wang, X., and Luo, Z.G. (2016). The hominoid-specific gene TBC1D3 promotes generation of basal neural progenitors and induces cortical folding in mice. Elife *5*, 1–25.

Kandyba, E., Leung, Y., Chen, Y.-B., Widelitz, R., Chuong, C.-M., and Kobielak, K. (2013). Competitive balance of intrabulge BMP/Wnt signaling reveals a robust gene network ruling stem cell homeostasis and cyclic activation. Proc. Natl. Acad. Sci. USA *110*, 1351–1356.

Kessaris, N., Fogarty, M., Iannarelli, P., Grist, M., Wegner, M., and Richardson, W.D. (2006). Competing waves of oligodendrocytes in the forebrain and postnatal elimination of an embryonic lineage. Nat. Neurosci. *9*, 173–179.

Lewitus, E., Kelava, I., and Huttner, W.B. (2013). Conical expansion of the outer subventricular zone and the role of neocortical folding in evolution and development. Front. Hum. Neurosci. *7*, 1–12.

Li, D., Takeda, N., Jain, R., Manderfield, L.J., Liu, F., Li, L., Anderson, S.A., and Epstein, J.A. (2015). Hopx distinguishes hippocampal from lateral ventricle neural stem cells. Stem Cell Res. *15*, 522–529.

Llorens-Bobadilla, E., Zhao, S., Baser, A., Saiz-Castro, G., Zwadlo, K., and Martin-Villalba, A. (2015). Single-cell transcriptomics reveals a population of dormant neural stem cells that become activated upon brain injury. Cell Stem Cell *17*, 329–340.

Lois, C., and Alvarez-Buylla, A. (1994). Long-distance neuronal migration in the adult mammalian brain. Science *264*, 1145–1148.

Morel, L., Chiang, M.S.R., Higashimori, H., Shoneye, T., Iyer, L.K., Yelick, J., Tai, A., and Yang, Y. (2017). Molecular and functional properties of regional astrocytes in the adult brain. J. Neurosci. *37*, 8706–8717.

Mühlfriedel, S., Kirsch, F., Gruss, P., Stoykova, A., and Chowdhury, K. (2005). A roof plate-dependent enhancer controls the expression of Homeodomain only protein in the developing cerebral cortex. Dev. Biol. *283*, 522–534.

Nakashima, K., Takizawa, T., Ochiai, W., Yanagisawa, M., Hisatsune, T., Nakafuku, M., Miyazono, K., Kishimoto, T., Kageyama, R., and Taga, T. (2001). BMP2-mediated alteration in the developmental pathway of fetal mouse brain cells from neurogenesis to astrocytogenesis. Proc. Natl. Acad. Sci. USA *98*, 5868–5873.

Obarzanek-Fojt, M., Favre, B., Kypriotou, M., Ryser, S., Huber, M., and Hohl, D. (2011). Homeodomain-only protein HOP is a novel modulator of late differentiation in keratinocytes. Eur. J. Cell Biol. *90*, 279–290.

Pollen, A.A., Nowakowski, T.J., Chen, J., Retallack, H., Sandoval-Espinosa, C., Nicholas, C.R., Shuga, J., Liu, S.J., Oldham, M.C., Diaz, A., et al. (2015). Molecular identity of human outer radial glia during cortical development. Cell *163*, 55–67.

Plikus, M.V., Mayer, J., de la Cruz, D., Baker, R.E., Maini, P.K., Maxson, R., and Chuong, C. (2008). Cyclic dermal BMP signaling regulates stem cell activation during hair regeneration. Nature *451*, 340–344.

Schuurmans, C., Armant, O., Nieto, M., Stenman, J.M., Britz, O., Klenin, N., Brown, C., Langevin, L.-M., Seibt, J., Tang, H., et al. (2004). Sequential phases of cortical specification involve Neurogenin-dependent and -independent pathways. EMBO J. *23*, 2892–2902.

Shin, C.H., Liu, Z., Passier, R., Zhang, C., Wang, D., Harris, T.M., Yamagishi, H., Richardson, J.A., Childs, G., Olson, E.N., et al. (2002). Modulation of cardiac growth and development by HOP, an unusual homeodomain protein. Cell *110*, 725–735.

Smart, I.H.M. (2002). Unique morphological features of the proliferative zones and postmitotic compartments of the neural epithelium giving rise to striate and extrastriate cortex in the monkey. Cereb. Cortex *12*, 37–53.

Song, J., McColl, J., Camp, E., Kennerley, N., Mok, G.F., McCormick, D., Grocott, T., Wheeler, G.N., and Munsterberg, A.E. (2014). Smad1 transcription factor integrates BMP2 and Wnt3a signals in migrating cardiac progenitor cells. Proc. Natl. Acad. Sci. USA *111*, 7337–7342.

Spassky, N., Merkle, F.T., Flames, N., Tramontin, A.D., García-Verdugo, J.M., and Alvarez-Buylla, A. (2005). Adult ependymal cells are postmitotic and are derived from radial glial cells during embryogenesis. J. Neurosci. *25*, 10–18.

Srinivas, S., Watanabe, T., Lin, C.S., William, C.M., Tanabe, Y., Jessell, T.M., and Costantini, F. (2001). Cre reporter strains produced by targeted insertion of EYFP and ECFP into the ROSA26 locus. BMC Dev. Biol. *1*, 4.

Takeda, N., Jain, R., LeBoeuf, M.R., Wang, Q., Lu, M.M., and Epstein, J.A. (2011). Interconversion between intestinal stem cell populations in distinct niches. Science *334*, 1420–1424.

Thomsen, E.R., Mich, J.K., Yao, Z., Hodge, R.D., Doyle, A.M., Jang, S., Shehata, S.I., Nelson, A.M., Shapovalova, N.V., Levi, B.P., et al. (2016). Fixed single-cell transcriptomic characterization of human radial glial diversity. Nat. Methods *13*, 87–93.

Tiberi, L., Vanderhaeghen, P., and van den Ameele, J. (2012). Cortical neurogenesis and morphogens: diversity of cues, sources and functions. Curr. Opin. Cell Biol. *24*, 269–276.

Tiveron, M.-C., Beclin, C., Murgan, S., Wild, S., Angelova, A., Marc, J., Coré, N., de Chevigny, A., Herrera, E., Bosio, A., et al. (2017). Zic-proteins are repressors of dopaminergic forebrain fate in mice and *C. elegans*. J. Neurosci. *37*, 10611–10623.

De Toni, A., Zbinden, M., Epstein, J.A., Ruiz i Altaba, A., Prochiantz, A., and Caille, I. (2008). Regulation of survival in adult hippocampal and glioblastoma stem cell lineages by the homeodomain-only protein HOP. Neural Dev. *3*, 13.

Tsai, H.-H., Li, H., Fuentealba, L.C., Molofsky, A.V., Taveira-Marques, R., Zhuang, H., Tenney, A., Murnen, A.T., Fancy, S.P.J., Merkle, F., et al. (2012). Regional astrocyte allocation regulates CNS synaptogenesis and repair. Science *337*, 358–362.

Wang, X., Tsai, J., LaMonica, B., and Kriegstein, A. (2011). A new subtype of progenitor cell in the mouse embryonic neocortex. Nat. Neurosci. *14*, 555–561.

Wang, L., Hou, S., and Han, Y.-G. (2016). Hedgehog signaling promotes basal progenitor expansion and the growth and folding of the neocortex. Nat. Neurosci. *19*, 888–896.

Winpenny, E., Lebel-Potter, M., Fernandez, M.E., Brill, M.S., Götz, M., Guillemot, F., and Raineteau, O. (2011). Sequential generation of olfactory bulb glutamatergic neurons by Neurog2-expressing precursor cells. Neural Dev. *6*, 12.

Yang, H.K.C., Sundholm-Peters, N.L., Goings, G.E., Walker, A.S., Hyland, K., and Szele, F.G. (2004). Distribution of doublecortin expressing cells near the lateral ventricles in the adult mouse brain. J. Neurosci. Res. *76*, 282–295.

Stem Cell Reports, Volume *11*

Supplemental Information

HOPX Defines Heterogeneity of Postnatal Subventricular Zone Neural Stem Cells

Stefan Zweifel, Guillaume Marcy, Quentin Lo Guidice, Deqiang Li, Christophe Heinrich, Kasum Azim, and Olivier Raineteau

Inventory of Supplemental Information

1) Supplementary experimental procedures
2) references related to experimental procedures
3) Supplementary figures S1 to S6 with legends

1) Supplementary Experimental Procedures

Plasmids

The following plasmids were used in this study: pCX-GFP (kind gift of X Morin, ENS, Paris; France); pFloxpA-DsRed express (kind gift of Colette Dehay; INSERM U1208, Bron, France); pCAG-Cre (Addgene; 13775); pCMV-Hopx (Open Biosystems; MMM1013-202767606); pPB-CAG-EmGFP (VB161220-1119syh; VectorBuilder Inc., Cyagen Bioscience, Santa Clara, California, USA); pCMV-hyPBase (kind gift of Laura López-Mascaraque; Instituto Cajal, Madrid, Spain). Plasmids were purified using the EndoFree Plasmid Kit according to the manufacturer's protocol (Qiagen; 12362). Plasmids were re-suspended to a final concentration of 5 µg/µl. Dorsal electroporations were performed in P1 to P2 (postnatal day 1 to 2) pups as previously described (Fernández et al., 2011). In $Hopx^{CreERT2}$ animals subcutaneous tamoxifen (Tam; SIGMA-Aldrich; T5648) administration (1 mg per pup) was performed 2 to 3 hrs after electroporation.

Primary Antibodies for Immunohistochemistry

The following primary antibodies were used for immunohistochemical procedures: Rabbit anti-Hopx (1:400; Santa Cruz; sc-30216); Mouse anti-Hopx (1:400; Santa Cruz; sc-398703); Goat anti-DCX (1:500; Santa Cruz; sc-8066); Mouse anti-Olig2 (1:1500; Millipore; MABN50); Mouse anti-GFAP (1:500; Millipore; MAB3402); Chicken anti-GFP (1:1000; AVES LABS; GFP-1020); Rabbit anti-RFP (1:1500; MBL; PM005); Rabbit anti-S100β (1:5000; SWANT); Chicken anti-βGal (1:4000; Abcam; ab9361); Goat anti-Mcm2 (1:300; Santa Cruz; sc-9839); Mouse anti-Sox2 (1:100; Santa Cruz; sc-365823); Rabbit anti-Blbp (1:300; Millipore; ABN14). Blocking was done in TNB buffer (0.1 M PB; 0.05% Casein; 0.25% Bovine Serum Albumin; 0.25% TopBlock) with 0.4% triton-X (TNB-Tx). Sections were incubated over night at 4°C with gentle shaking the following primary antibodies in TNB-Tx. Following extensive washing in 0.1 M PB with 0.4% triton-X (PB-Tx), sections were incubated with appropriate secondary antibodies conjugated with Alexafluor 488, 555 or 647 (1:500; Life Technologies) for 2 hrs at room temperature. Sections were washed and counterstained with Dapi (1:5000; Life Technologies; D1306). To increase the signal from YFP and βGal, biotinylated secondary antibodies (1:500; Jackson) were used in combination with DTAF conjugated streptavidin (1:250; Jackson) or a TSA amplification kit according to manufacturer's protocol (Life Technologies; T-20932), respectively.

FACsorting and qPCR

Hes5::EGFP (with C57BL/6 background) of the age P2-P4 were used for sorting for NSCs as previously described and using the exact same parameters (Azim et al. 2015). 4 to 5 animals of one litter was used for 1 "n" number. Microdissection of SVZ domains (dorso-medial; dorso-lateral and lateral) was performed in RNase free, sterile conditions. Microdissection of SVZ domains (dorso-medial; dorso-lateral and lateral) was performed in RNase free, sterile conditions. Tissues were dissociated using a trypsin-based Neural

Dissociation Kit (Miltenyi Biotec, Bergisch Gladbach, Germany). For additional purification of the Hes5-EGFP population, an APC conjugated NSC antibody against the transmembrane-protein prominin-1 (1:100; ebiosciences) was applied for 15 mins at RT, before suspension was subjected to Fluorescence Activated Cell Sorting (FACS Aria III; BD Bioscience, Franklin Lakes, New Jersey, USA). Dead cells were excluded by forward and sideward scatter. Gating settings were gained using an EGFP- wildtype animal and a prominin-1 isotype control conjugated to APC (rat anti-IgG; 1:100, ebiosciences). Brightest 30% of $EGFP^+$ cells, which where prominin-1^+ were collected directly into RNA lysis buffer and snap-frozen for further gene expression analysis. RNA extraction was performed using the RNeasy microkit (Qiagen; 74004) following manufacturer's guidelines. RNA amplification of 3 ng input material was done using the Nugene Pico Ovation WT kit (NuGen Technologies, Inc., San Carlos, CA) as described previously (Azim et al. 2015). qPCR was performed according to the procedures described elsewhere (Azim et al., 2012b, Azim et al., 2014b), with the LightCycler 480 (Roche, Basel, Switzerland). All reactions were performed in duplicates or triplicates and GAPDH was used as reference gene. Primers used were custom made by Qiagen (EGFP, Eomes, Hopx, Pcna, Sp8) or designed with the Primer Express 1.5 software and produced by Eurofins (Schönenwerd, Switzerland):

GAPDH:	fw_CGTCCCGTAGACAAAATGGT,	rv_TTGATGGCAACAATCTCCAC;
Aldh1l1:	fw_CAGTAAACCTCCTGGCCAAA,	rv_CCCTGTTTTCCCTACTTCCC;
Aqp4:	fw_TGAGCTCCACATCAGGACAG,	rv_TCCAGCTCGATCTTTTGGAC;
Dct:	fw_GCATCTGTGGAAGGGTTGTT,	rv_ACTCCTTCCTGAATGGGACC;
DCX:	fw_CTGACTCAGGTAACGACCAAGAC,	rv_TTCCAGGGCTTGTGGGTGTAGA;
Dlx2:	fw_CTTCTTGAACTTGGATCGGC,	rv_AGACCCAGTATCTGGCCCTG;
Ebf1:	fw_GGTGGAAGTCACACTGTCGTAC,	rv_GTAACCTCTGGAAGCCGTAGTC;
Fgfr3:	fw_ACAGGTGGTCATGGCAGAAGCT,	rv_CTCCATCTCAGATACCAGGTCC;
Gli1:	fw_CTCAAACTGCCCAGCTTAACCC,	rv_TGCGGCTGACTGTGTAAGCAGA;
Gli3:	fw_CGAGAACAGATGTCAGCGAG,	rv_TGAGGCTGCATAGTGATTGC;
Hes5:	fw_GTAGTCCTGGTGCAGGCTCT,	rv_AACTCCAAGCTGGAGAAGGC;
Id3:	fw_GCGTGTCATAGACTACATCCTCG,	rv_GTCCTTGGAGATCACAAGTTCCG;
Lef1:	fw_CGTCACACATCCCGTCAGATGTC,	rv_TGGGTGGGGTGATCTGTCCAACG;
Olig1:	fw_AGCAAGCTCAAACGTTGGTT,	rv_GTTCTGTTTTTCAGGCTCGC;
Olig2:	fw_GACGATGGGCGACTAGACA,	rv_CAGCGAGCACCTCAAATCTA;
PDGFRα:	fw_AGAAAATCCGATACCCGGAG,	rv_AGAGGAGGAGCTTGAGGGAG;
Plp1:	fw_GGGCCCCTACCAGACATCTA,	rv_TCCTTCCAGCTGAGCAAAGT;
Tcf7:	fw_TGCCTTCAATCTGCTCATGCC,	rv_GTGTGGACTGCTGAAATGTTCG;
Vax1:	fw_CTCTACAGGCTGGAGATGGAGT,	rv_GCTTAGTCCGCCGATTCTGGAA.

Meta-analysis of Transcriptional Profiles

To generate the lists of TFs that are enriched in dNSCs and lNSCs, we made use of our recently published transcriptional datasets (Azim et al., 2015; GSE60905). We analyzed the dataset on the "Gene Expression Omnibus" (https://www.ncbi.nlm.nih.gov/geo/) for transcripts that are differentially expressed between dNSCs and lNSCs (≥1.8 fold enrichment and p-values <5%). Finally, we selected transcripts for transcription factor activity and regulation of transcription using "DAVID Analysis Wizard" (https://david.ncifcrf.gov/). Lists of

transcripts were analyzed for enrichments in the neuronal, astrocytic or oligodendrocytic lineage using the transcriptional dataset of the Barres group (Cahoy et al., 2008; GSE9566). Heatmaps were produced using a self-made R script “Heatmap Generator”, which enables us to compare and generate heatmaps from different datasets available via the “Gene Expression Omnibus” (GEO).

2) REFERENCES

Azim, K., Raineteau, O., and Butt, A.M. (2012). Intraventricular injection of FGF-2 promotes generation of oligodendrocyte-lineage cells in the postnatal and adult forebrain. Glia *60*, 1977–1990.

Azim, K., Fischer, B., Hurtado-Chong, A., Draganova, K., Cantù, C., Zemke, M., Sommer, L., Butt, A., and Raineteau, O. (2014). Persistent Wnt / b -Catenin Signaling Determines Dorsalization of the Postnatal Subventricular Zone and Neural Stem Cell Specification into Oligodendrocytes and Glutamatergic Neurons. Stem Cells *23*, 1301–1312.

Azim, K., Hurtado-Chong, A., Fischer, B., Kumar, N., Zweifel, S., Taylor, V., and Raineteau, O. (2015). Transcriptional Hallmarks of Heterogeneous Neural Stem Cell Niches of the Subventricular Zone. Stem Cells *33*, 2232–2242.

Cahoy, J.D., Emery, B., Kaushal, A., Foo, L.C., Zamanian, J.L., Christopherson, K.S., Xing, Y., Lubischer, J.L., Krieg, P.A., Krupenko, S.A., et al. (2008). A Transcriptome Database for Astrocytes , Neurons , and Oligodendrocytes : A New Resource for Understanding Brain Development and Function. J. Neurosci. *28*, 264–278.

Fernández, M.E., Croce, S., Boutin, C., Cremer, H., and Raineteau, O. (2011). Targeted electroporation of defined lateral ventricular walls: a novel and rapid method to study fate specification during postnatal forebrain neurogenesis. Neural Dev. *6*, 13.

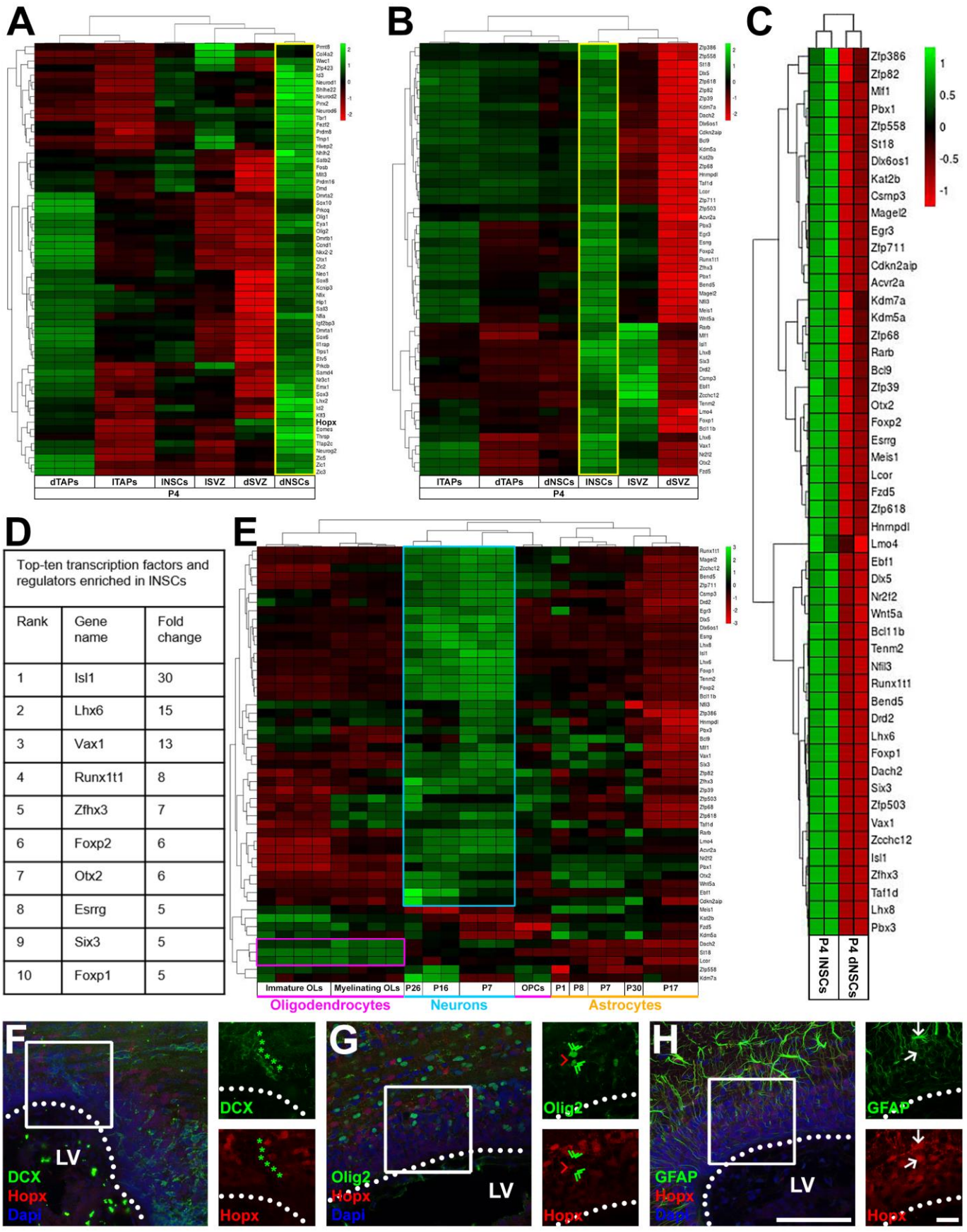

Rank	Gene name	Fold change
1	Isl1	30
2	Lhx6	15
3	Vax1	13
4	Runx1t1	8
5	Zfhx3	7
6	Foxp2	6
7	Otx2	6
8	Esrrg	5
9	Six3	5
10	Foxp1	5

Figure S1. Analysis of TFs enriched in regionally separated NSC population. Related to Figure 1

(A, B): Heatmaps confirming the enrichment of selected TF transcripts in dNSC (vs. lNSCs; A) and lNSCs (vs. dNSCs; B), including the transcriptional profile in TAPs and the environment (SVZ) of those two regions. **(C):** Heatmap of in P4 lNSCs enriched TFs compared to their dorsal counterparts (≥1,8 folds and p-value<0,05).

(D): List of the top ten TFs enriched in lNSCs.

(E): Lineage-specific meta-analysis of lNSC TFs using the dataset from the Barres group: oligodendrocytes (purple, 3/51); astrocytes (yellow, 0/51); neurons (turquoise, 42/51).

(F-H): Confirmation of astroglial lineage-specific enrichment of Hopx by immunohistochemistry within the SVZ. Hopx is absent from neuroblasts (DCX, F) and OPCs (Olig2, G), but is observed in astrocytes (GFAP, H).

Scale bars: H (overview) = 100 µm; H (crops) = 25 µm.

Abbreviations: dTAPs, dorsal transient amplifying progenitors; lTAPs, lateral transient amplifying progenitors; dNSCs, dorsal NSCs; lNSCs, lateral NSCs; dSVZ, dorsal SVZ; lSVZ, lateral SVZ; oligodendrocyte precursor cells, OPCs; OL, oligodendrocyte; LV, lateral ventricle.

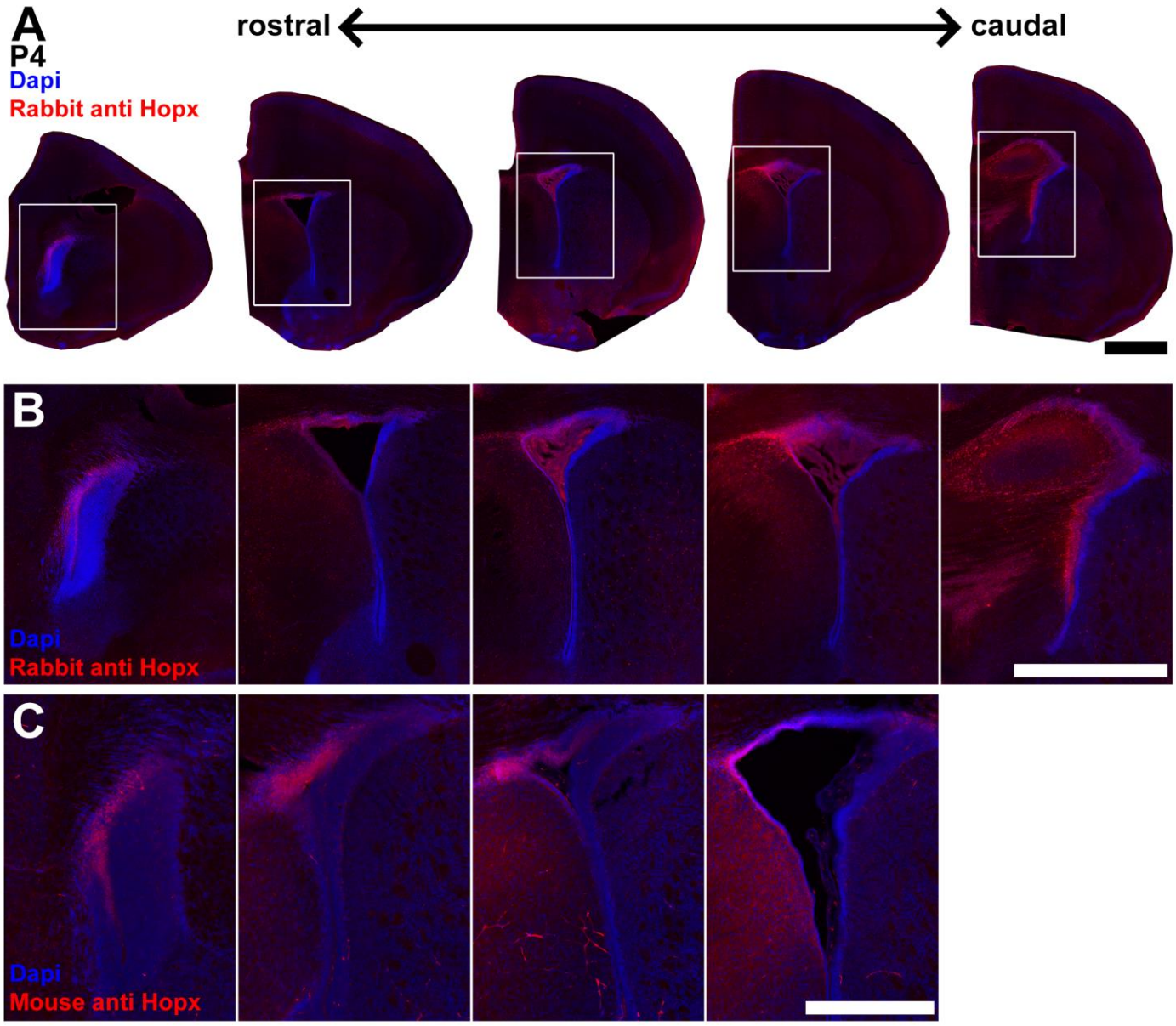

Figure S2. Spatial heterogeneity of Hopx expression at P4. Related to Figure 2

(A-C): Representative pictures demonstrate Hopx expression in a P4 animal along the rostro-caudal axis. The top and middle panel show overviews (A) and higher magnification pictures (B) of tissue stained with the rabbit anti Hopx antibody. The bottom panel shows higher magnification pictures of tissue stained with the mouse anti Hopx antibody (C). Note that both antibodies exhibit the same spatial pattern of Hopx expression. Scale bars: A, B = 1 mm; C = 500 µm.

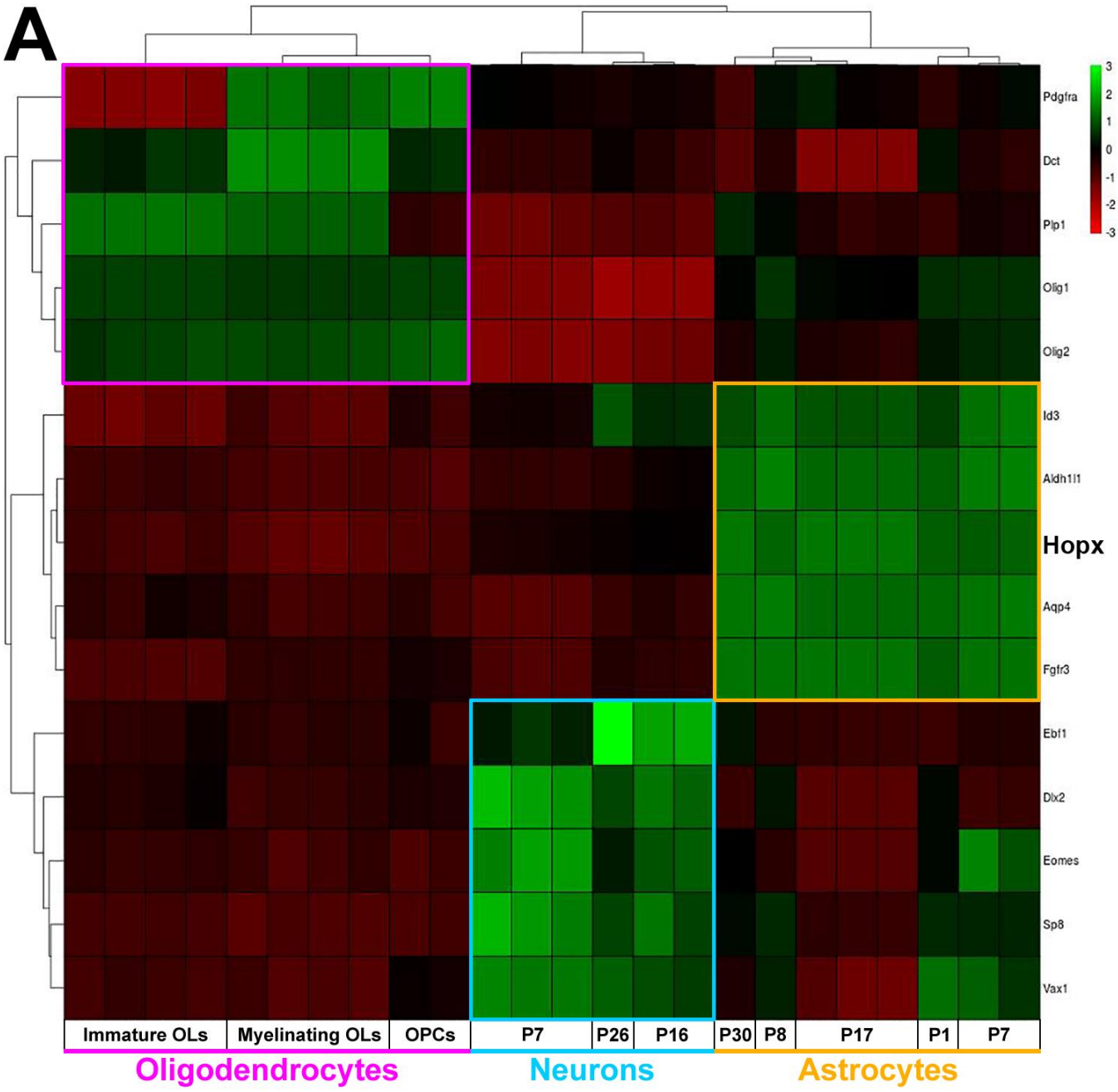

Figure S3. Confirmation of lineage specificity of selected transcripts using the dataset from the Barres group. Related to Figure 3

5 transcripts of the oligodendrocytic lineage (*PDGFRa, Dct*, *Plp1, Olig1, Olig2*), 5 of the neuronal lineage (*Ebf1, Dlx2, Eomes, Sp8, Vax1*) and 5 of the astrocytic lineage (*Id3, Aldh1l1, Hopx, Aqp4, Fgfr3*) were selected.

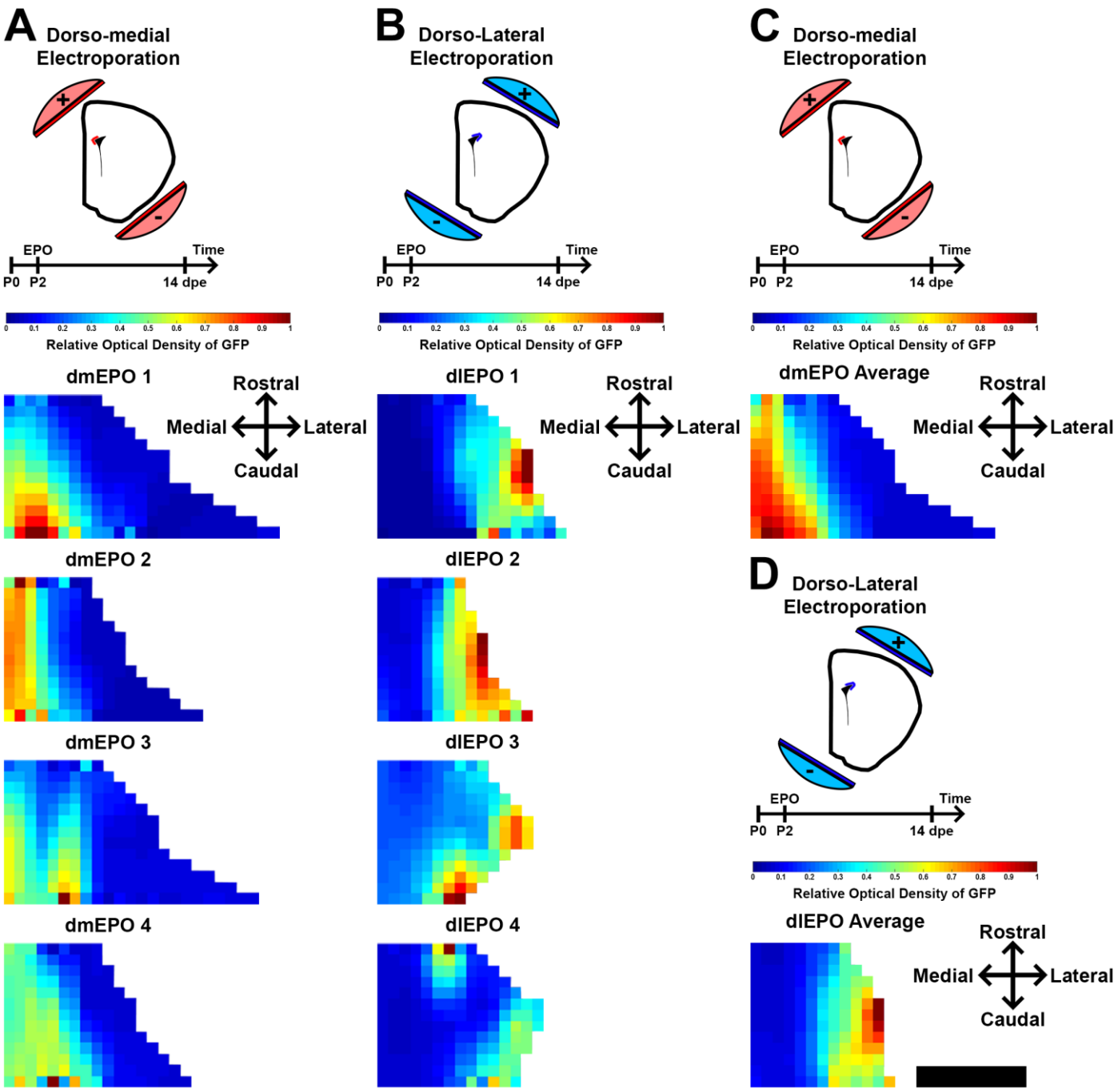

Figure S4. Optical density measurements of GFP reveal the high efficiency of targeted dorso-medial and dorso-lateral EPO. Related to Figure 3

(A+B): Heatmaps representing the relative optical density of GFP expression in the dorsal SVZ of different individuals following dorso-medial (A) or dorso-lateral EPO (14 dpe; B). Heatmaps are color coded (0 = dark blue; highest measured value = dark red). Heatmap orientation is: left = rostral; right = caudal; top = medial; bottom = lateral.

(C+D): Heatmaps representing the averaged values of 4 animals those received dorso-medial (C) or dorso-lateral EPO (D).

Animals: dmEPO, n=4; dlEPO, n=4.

Scale bar: D = 500 µm

Abbreviations: dpe, days post electroporation; EPO, electroporation; dmEPO, dorso-medial electroporation; dlEPO, dorso-lateral electroporation; SVZ, subventricular zone.

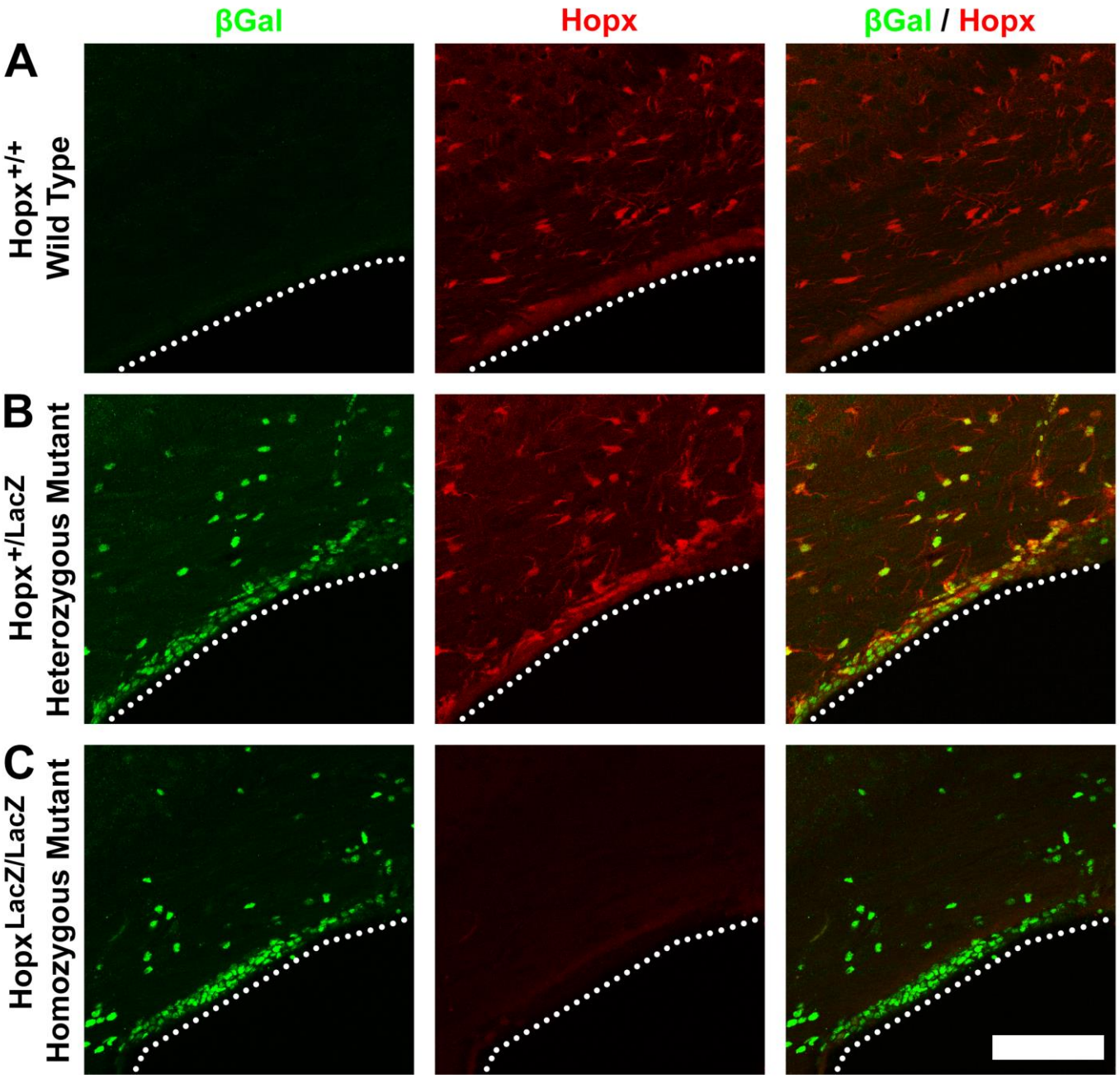

Figure S5. The Hopx$^{LacZ/WT}$ knockin transgenic mouse line. Related to Figure 5

(A-C): Co-stainings of βGal and Hopx were performed in Hopx$^{WT/WT}$ (A), Hopx$^{WT/LacZ}$ (B) and Hopx$^{LacZ/LacZ}$ (C) animals. Representative micrographs confirm the absence of βGal in Hopx$^{WT/WT}$ (A) and Hopx in Hopx$^{LacZ/LacZ}$ (C) animals, while Hopx$^{WT/LacZ}$ animals co-express both genes in the dSVZ, as well as CC (B).

Scale bar: 100 µm.

Abbreviations: βGal, β-galactosidase; dSVZ, dorsal SVZ; CC, corpus callosum; WT, wild type.

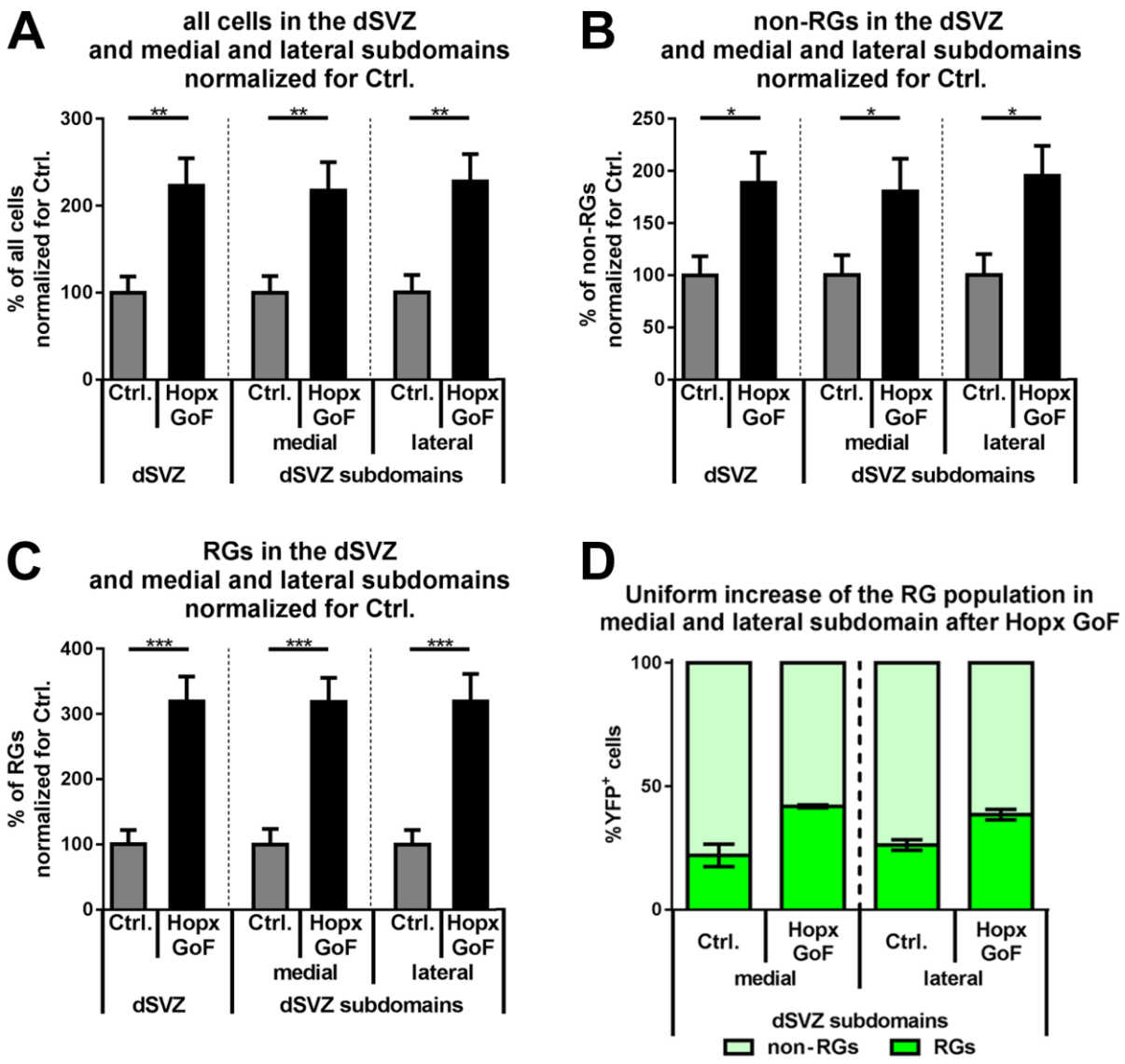

Figure S6. No difference in enlargement of the population after Hopx overexpression along the dSVZ. Related to Figure 6

(A-C): Full population (A), non-RG cells (B) and RG (C) are increased 4 days following Hopx overexpression. No difference in the enlargement between the medial and the lateral subdomain of the dSVZ was observed. Graphs are presented in percentage of the change normalized for control.

(D): The fractions of the RG population were equally increased in the medial and the lateral subdomain of the dSVZ following Hopx GoF.

Animals: Ctrl., n=7; GoF, n=5.

Abbreviations: Ctrl., control; dSVZ, dorsal SVZ; GoF, gain of function; RG, radial glia.